Large-scale Climate and Atmospheric Drivers of Local Headland Bypassing

A. P. Silva[1,2], G. Vieira da Silva[1], P. Gomes da Silva[3], D. Strauss[1], R. Tomlinson[1]

[1]Coastal and Marine Research Centre, Griffith University, Gold Coast campus – G51, QLD 4222, Australia.

[2]School of Engineering and Built Environment, Griffith University, Gold Coast campus, Australia.

[3]IHCantabria – Instituto de Hidráulica Ambiental de la Universidad de Cantabria, Santander, Spain.

Corresponding author: Ana Paula da Silva (ana.dasilva@alumni.griffithui.edu.au)

Key Points:

- Strong low-pressure systems situated near the coast between 25 and 35ºS have the potential to trigger headland bypassing around Fingal Head.
- Slight changes in storm wave conditions generated by these atmospheric patterns can trigger different formats and magnitude of bypassing pulses.
- Large-scale climate drivers influence the long-term cycles of bypassing through controlling the longshore transport and updrift sediment availability.

Abstract

Headland Bypassing is mainly a wave-driven coastal process that interconnects sediment compartments and allows the continuity of the longshore sediment transport. In turn, waves are subject to atmospheric patterns and climate drivers. Hence, this study focuses on identifying the atmospheric systems and associated wave conditions that have triggered bypassing events in Fingal Head (New South Wales, Australia) over last 33 years. For this, clustering techniques were used to identify 225 weather types that represent the daily atmospheric variability over the Coral-Tasman Seas. Four recent storm events that triggered headland bypassing were numerically simulated including waves, currents, sediment transport and morphological evolution in order to identify the relevant weather types for the development of the sand pulse. Results revealed that strong low-pressure systems (e.g., Tropical Cyclones and East Coast Lows) occurring off the Eastern Australian coast around 30°S are the dominant patterns triggering bypassing events in the study area. The headland bypassing mechanism was observed to vary between large sandbar system and sediment leaking around the headland according to slight changes in the sea states generated by these storm events. Overall, atmospheric patterns showed control over when and how the bypassing pulse occurs, whereas sediment availability is the main factor influencing long-term cycles of bypassing that are subject to the variability of El Niño – Southern Oscillation and Pacific Decadal Oscillation. Altogether, this study emphasized the intricacy between the multiple factors controlling headland bypassing events, which has direct implications on the potential for predicting the occurrence of this local coastal process.

Plain Language Summary

The movement of sand along the coast is at times constrained by the presence of headlands. Headland bypassing is the natural process of sediment moving around a coastal rocky outcrop influenced by the wave action. On the other hand, waves are influenced by atmospheric pressure systems and these, in turn, are influenced by global climate oscillations. Hence, in this study the atmospheric patterns that prevail over the Coral-Tasman Sea are investigated and, consequently, how these synoptic scale systems modulate the sand movement around Fingal Head (New South Wales, Australia) over the last 33 years. The results demonstrate that storms such as Tropical Cyclones and East Coast Lows approaching latitude 30°S have the potential to generate waves that promote sand movement around Fingal Head. It is also evident that the amount of sand available on the beach south of the headland is relevant for longer cycles of bypassing. Overall, understanding and predicting the periods when sand movement will be occurring around headlands is a complex task that requires detailed research of several physical factors. For Fingal Head, this study demonstrates that the variability of the sand volume is associated with globally important climate indices such as El Niño – Southern Oscillation, which has dictated the multiple years periods of headland bypassing.

1 Introduction

Shoreline research around the world has grown expressively over the last few years and with it, the development of a direct relation between large-scale climate systems and coastline variability at multiple temporal and spatial scales (e.g., Barnard et al., 2015; Castelle et al., 2015; Harley et al., 2017; Wiggins et al., 2020; Silva et al., 2020; 2021a; Vos et al., preprint). The connection, however, between global climate drivers and shoreline position relies on a series of intermediary nearshore processes, for which there is still a deficiency of knowledge in terms of their particular

response to climate patterns variability (Graffin et al., preprint). While adding these local-scale dynamical processes and non-linear interactions increases the complexity of the shoreline analysis, they also represent a valuable contribution to refine predictions at a local-level (Short, 2022; Harley et al., 2022).

As one of the main drivers of shoreline changes, waves have been largely studied and frequently associated with climate indices (Montaño et al., 2020; Odériz et al., 2020; Graffin et al., preprint). It is well-defined now, for instance, that the El Niño-Southern Oscillation (ENSO) has a prominent influence on wave climate and shoreline variability across the globe from interannual to multidecadal timescales (Odériz et al., 2020; Graffin et al., preprint). Throughout the Pacific Ocean, in particular, ENSO controls multiple atmospheric systems and oceanic conditions (e.g., wave energy and direction) that impact on coastal vulnerability (Barnard et al., 2015; Anderson et al., 2018; Vos et al., preprint). On the other hand, uncertainties are still pronounced in terms of the subaqueous variability of the beach profile and the sediment migration along the coast in response to changes in these regional weather patterns and global climate oscillations. Among the few studies investigating the influence of atmospheric and climate patterns on sediment transport, Splinter et al. (2012) observed that changes to the net longshore transport over 50 years (1958 – 2009) on the East Australian Coast were strongly related to ENSO and the Interdecadal Pacific Oscillation (IPO). This relationship was most significant during negative IPO and La Niña phases which led to more southerly deviations in the net northward longshore sediment transport. Also in Eastern Australia, Ribo et al. (2020) extended the knowledge on longshore transport to the millennial-scale, suggesting that the net northward littoral drift was impacted by latitudinal shifts of the Subtropical Ridge controlling the directional wave climate. Moreover, the study noticed the additional relevance of headlands in controlling the regional longshore transport under the distinct sea-level and wave conditions over multi-centennial periods.

Effectively, headlands act like a valve that intermittently allows sediment migration downdrift (Klein et al., 2020), a coastal process called headland bypassing (HB). The ability (or not) of sand to bypass a headland has evident importance since it controls the sediment budget of the downdrift beach compartment (Thom et al., 2018, Goodwin et al., 2020). This subaqueous movement of sand around a headland in the direction of the longshore drift is complex and depends on several controlling factors. These include the geometry of the headland and nearshore bathymetry (George et al., 2015; King et al., 2021), sediment characteristics and availability (Cascalho et al., 2014; Ribeiro, 2017; George et al., 2019), and hydrodynamic drivers such as tides (McCarroll et al., 2018; Costa et al., 2019; Valiente et al., 2019) and above all, waves (Ab Razak, 2015, Vieira da Silva et al., 2016a,b; 2018a; 2021; King et al., 2019; 2021; Wishaw et al., 2021). The influence of wave characteristics in conditioning the occurrence of a headland bypassing event recalls the importance of the large-scale atmospheric patterns and climate drivers that induce the regional variability of the wave generation, impacting the sediment transport along the coast and, at last, the shoreline.

A substantial obstacle to developing a connection between HB cycles and climate variability is the lack of long-term real-world measurements. Field surveys around headlands and within the surf zone are limited due to the hazardous environmental conditions and the restricted access to specific equipment and trained personnel (McCarroll et al., 2018; Klein et al., 2020). On the other hand, remote sensing techniques have recently increased their potential as tools to derive

coastal measurements with the number of satellites multiplying and the imagery resolution improving significantly. As a result, only a few studies so far were able to derive some sort of relationship between bypassing and climate indices. Using three temporally sparse bathymetric surveys (1883, 2002 and 2011), Goodwin et al. (2013) describes the HB mechanism around Cape Byron (Australia) and suggests that the IPO influences the wave climate in decadal scale which leads to shifts in the bypassing pathways. Then, based on aerial imagery spanning 60 years, Wishaw et al. (2021) observed that the completion of HB cycles required a specific sequence of wave conditions and that the neutral to La Niña phases would support the sand movement around Noosa Headland (Australia). Lastly, Silva et al. (2021a) acquired detailed topo-bathymetric surveys that covered a full bypassing cycle triggered by a Tropical Cyclone in the Northern New South Wales coast (Fingal Head, NSW - Australia) in February 2019. After developing a conceptual model of the mechanism, the frequency of occurrence of bypassing events was investigated using satellite-derived shorelines which revealed multi-annual to decadal cycles likely related to the oscillations in ENSO and the Pacific Decadal Oscillation (PDO) phases (Silva et al., 2021a).

Exploring further the headland bypassing dataset provided by Silva et al. (2021a), the present study investigates the relationship between weather patterns over the Coral and Tasman Seas and the sediment transport around Fingal headland in the Eastern Australia Coast over the last 33 years, including the identification of specific storm types that have triggered bypassing pulses. The susceptibility of this local-scale coastal process to the variability of global climate drivers such as El Niño Southern Oscillation (ENSO) and Pacific Decadal Oscillation (PDO) is also assessed. Finally, a discussion of how the findings of this study would inform future bypassing predictions is provided.

2 Regional Settings

The study area is situated in Fingal Head (Tweed Heads, NSW - Australia) and adjacent beaches: Dreamtime Beach on the updrift and Fingal Beach on the downdrift of the headland (Figure 1c). This headland as well as Cook Island (600 m offshore, Figure 1c) and Nine Mile Reef, extending 7 km offshore off the island are formed of basalt rock from the Tertiary Period (Fox, 2016). Fingal Head has about 20 m of elevation and a perimeter of about 700 m. The headland is asymmetric with about 90% of its area on the updrift side of the apex. The apex angle is approximately 80º and it is diagonally (22º, 300 m distance) aligned with the submerged rocky reef extending onshore from Cook Island. The surrounding bathymetry of Fingal Head is around -5 m AHD (Australian Height Datum) and the regional depth of closure is approximately -14 m AHD (Strauss et al., 2013). Both updrift and downdrift beaches are formed by fine quartzose sand (approximate d50 ~0.2 mm) (Chapman, 1981). The sediment input for this region is part of the northward littoral drift within the primary central-east coast compartment that extends from Clarence River in the south to the Tweed River in the north (Short, 2019; Thom et al., 2018) and beyond.

This section of the coast is classified as wave-dominated, with open coast beaches predominantly double barred (Short, 2019), a formation frequently observed at Dreamtime Beach. The wave climate in this region is dominated by a south-southeast (S-SE) swell with average significant wave height (Hs) of 1.5 m and peak period (Tp) of 10 s (Allen and Andrews, 1997). At the Tweed Wave Buoy location (Figure 1a), modal wave conditions vary between 8 and 12 s Tp with about 1 to 1.5 m Hs, and persistent easterly (E) to E-SE wave direction (Vieira da Silva et

al., 2017). These wave characteristics influence the longshore current direction towards north, transporting a net average of 500,000 m^3 every year (Patterson, 2007). Finally, in terms of local water level, the study area is in a semi-diurnal microtidal region (Chapman, 1981) with a tidal range of 1.45 m.

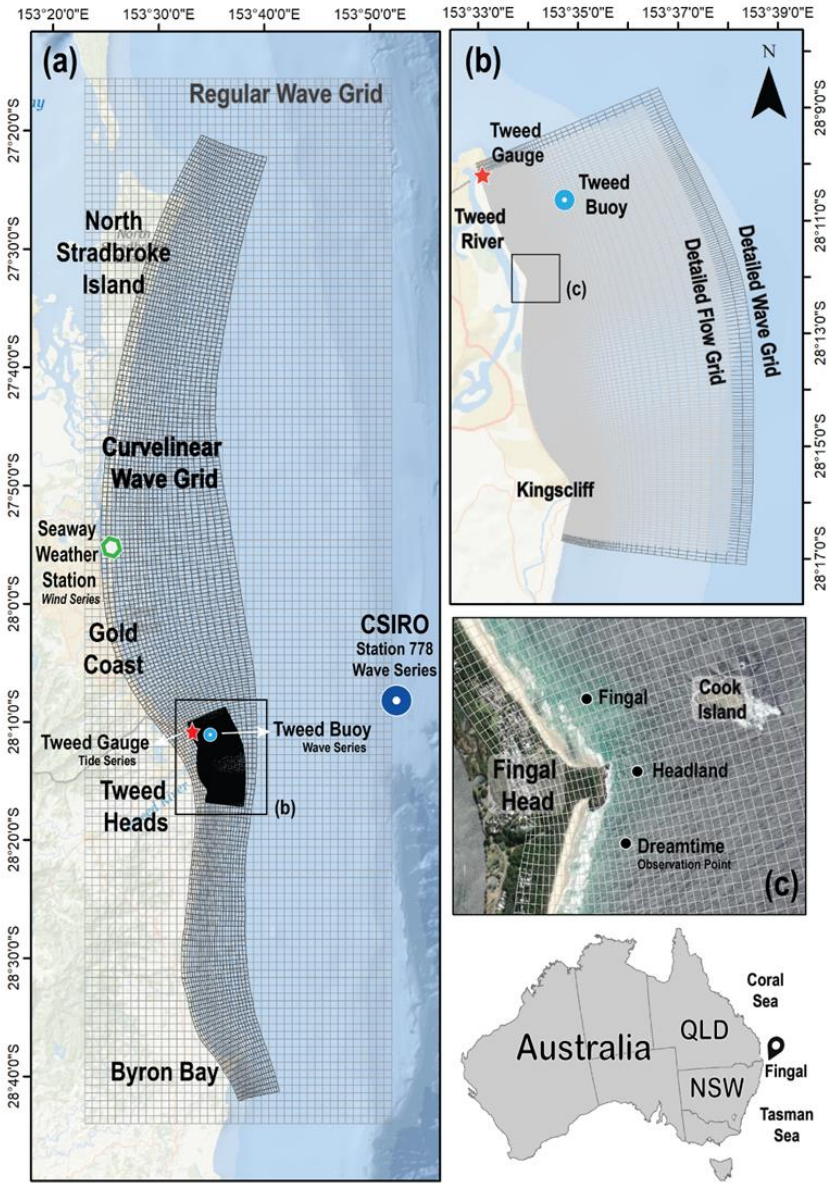

Figure 1. Study Area. (a) Regional view of the study area extending from the northern end of New South Wales (NSW) to Southeast Queensland (QLD). Wave modelling regional grids are represented covering the region from Byron Bay (NSW) to North Stradbroke Island (QLD) and extending offshore to the wave input station. (b) Local wave and flow grids are represented as well as the position of the Tweed Wave Buoy and Tweed River tide gauge. (c) presents a zoomed view of Fingal Head and Cook Island as well as the observations points at Dreamtime beach (updrift of the headland), at Fingal Beach (downdrift of the headland) and in front of Fingal Head.

Investigating the energy source areas and travel time of the waves reaching the region between North Stradbroke Island (Queensland) and Cape Byron (New South Wales (see Figure 1a for location), Silva et al. (2021b) identified that waves generated up to the periphery of the Coral-Tasman Seas (about 3 days travel time) are the main components of the wave climate for the study area. A large variety of atmospheric systems within the Coral-Tasman Seas is observed to influence the wave generation zones (Shand et al., 2010), including anticyclonic intensification, Tropical Cyclones, Tropical Lows, East Coast Lows and Southern Tasman Lows (Mortlock and Goodwin, 2015). The seasonal migration of the high-pressure anticyclones dictates the synoptic systems variability along the coast (Drosdowsky, 2005). During austral summer and autumn, the Tropical Cyclones and Lows are formed over the warm waters of the Coral Sea and enhance the generation of waves that reach the study area from the E-NE (Silva et al., 2021b). These tropical storms propagate waves to the study region with Hs up to 7 – 8 m (Shand et al., 2010; Vieira da Silva et al., 2018b). On the other hand, during austral winter months, the strong low-pressure systems over the Tasman Sea increase the wave component from the S-SE (Mortlock and Goodwin, 2015; Silva et al., 2021b).

The wave generation zones' variability has also been associated with large-scale climate drivers such as ENSO. Several studies observed El Niño (La Niña) phases leading to modal and extreme wave conditions from S-SE (E-NE) along the Tasman Sea coast (Harley et al., 2010; Hemer et al., 2010; Mortlock and Goodwin 2015). Silva et al. (2021b) identified an intensification in wave generation zones within the Coral-Tasman Sea during La Niña events, increasing the potential coastal hazards for the Eastern Australian Coast during these periods (Odériz et al., 2020). In terms of variability of atmospheric patterns due to ENSO events, a strong relationship has been previously reported for Tropical Cyclone migration towards Southeast Queensland under the influence of La Niña conditions (Chand et al., 2019); however, there is no clear evidence of ENSO events controlling the variability of East Coast Lows and similar atmospheric systems (Dowdy et al., 2019), despite the reported influence on the southerly wave component (Mortlock and Goodwin 2015).

3 Materials and Methods

To achieve the aims of this research, the methods were divided into two major steps (Figure 2): (1) the weather type analysis linking the sea-state parameters (predictand) to the wave-generating synoptic-scale atmospheric systems (predictor) and their temporal variability; then, the results from the weather type assessment were used to inform (2) the process-based numerical modelling of local wave conditions, longshore sediment transport and beach morphology variability.

3.1. Dataset

3.1.1. Atmospheric Data

Mean sea level pressure (SLP) fields were obtained from the US National Center for Environmental Prediction (NCEP) Climate Forecast System (CFS) Reanalysis versions 1 and 2 (CFSv1 and CFSv2) (Saha et al., 2010; 2014) and used in the weather type analysis (Figure 2). The CFSR is a third-generation global reanalysis with a high–resolution coupled atmosphere–ocean–land surface–sea ice system developed to provide the estimate of the state of these coupled domains over a period of time. The reanalysis series extends from 1979 to 2010 for the

CFSv1 and from 2011 to the present for the upgraded CFSv2. The SLP fields are available at an hourly time resolution and a horizontal resolution of 0.5° latitude × 0.5° longitude.

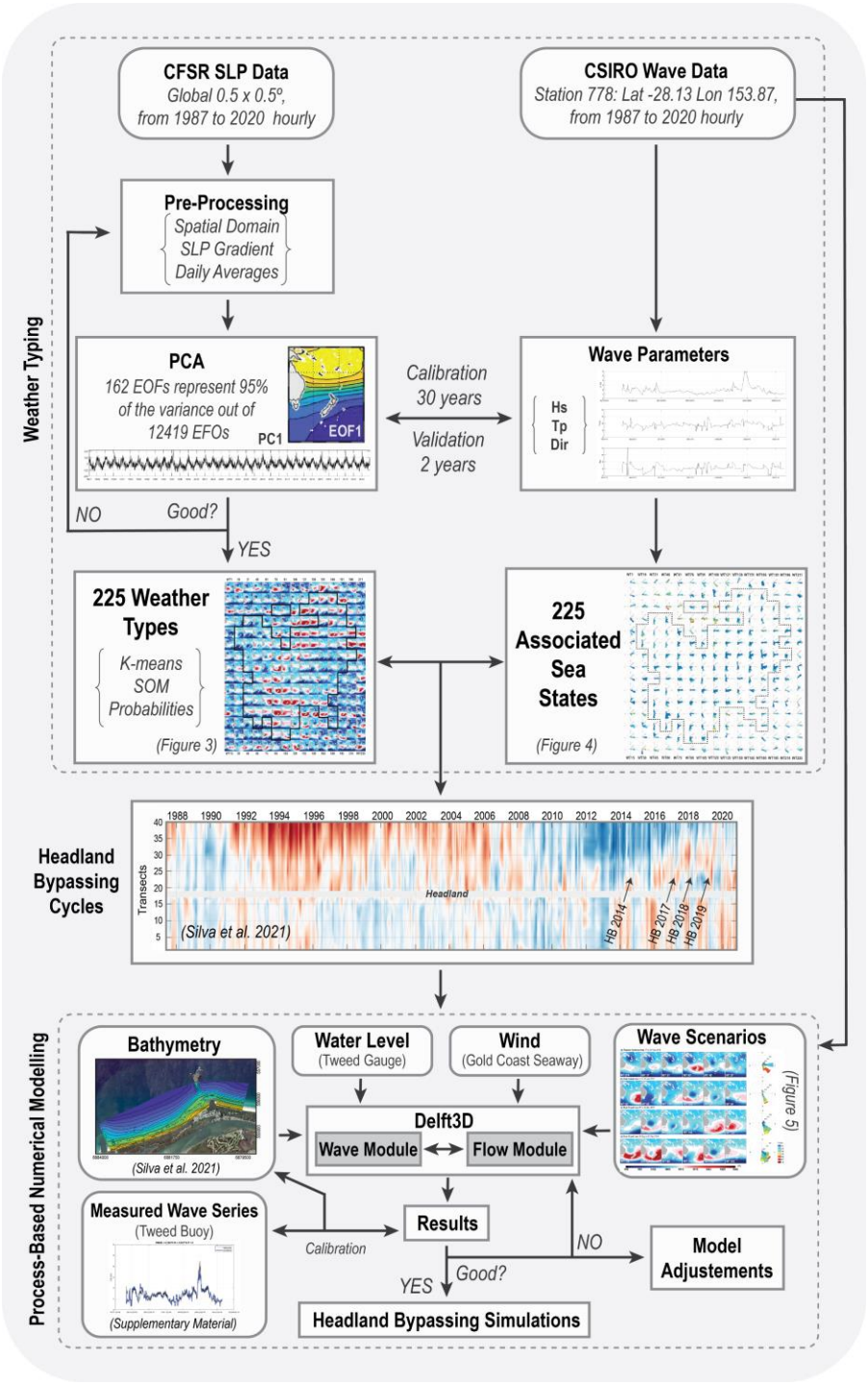

Figure 2. Framework of the methodology applied in this study. The first section, delimited by the grey dashed line, presents the steps for the weather analysis. After identifying the weather types, four storm events that have triggered HB are selected based on Silva et al. (2021a) results. The selected events are then modelled as presented in the last dashed area.

223 3.1.2. Wave data

224 Wave data was obtained from the CAWCR wave hindcast (Durrant et al., 2019). This dataset
225 was generated using the WaveWatch III v4.08/v4.18, wave model forced with NCEP CFSR
226 hourly winds and daily sea ice (Durrant et al., 2019). The dataset contains 3683 points within a
227 global grid of 0.4 degree (Durrant et al., 2019). The time series from a point (station 778) located
228 34-km offshore of the Tweed coast (NSW, Australia) (28.13ºS, 153.9ºE) was selected to be used
229 in this study (Figure 1). Wave parameters such as significant wave height (Hs), peak period (Tp)
230 and peak direction (Dirp) are available hourly within a time series that covers from 01 January
231 1987 to 31 December 2020.

232 3.1.3. Climate Index data

233 Climate indices were used to support the investigation of the variability of weather types in
234 relation to the different flavours of these large-scale drivers. Both the Southern Oscillation Index
235 (SOI) and the Pacific Decadal Oscillation (PDO) series were obtained from NCDC/NOAA
236 (https://www.ncdc.noaa.gov/teleconnections). The SOI index represents the El Niño-Southern
237 Oscillation (ENSO) variability, which indicates El Niño (La Niña) events for negative (positive)
238 SOI phases based on the standardized difference of monthly average sea-level pressure between
239 Tahiti (French Polynesia) and Darwin (Australia). The Pacific Decadal Oscillation (PDO) series
240 also oscillates between positive (El Niño-like) and negative (La Niña-like) phases, based on the
241 sea-surface temperature anomalies in the northeast and tropical Pacific Ocean. In this study, a
242 threshold of ±1 was used to characterize the climate index anomalies that indicate ENSO and
243 PDO phases.

244 3.2. Weather Typing

245 There are several approaches to estimate the relationship between atmospheric patterns and wave
246 conditions. A less computationally expensive is the weather-type method that uses clustering
247 techniques to classify atmospheric pressure fields into groups that can be statistically associated
248 to wave parameters (Giorgi et al., 2001; Caires et al., 2006; Costa et al., 2020). Camus et al.
249 (2014) proposed and validated a framework that consists of grouping the atmospheric circulation
250 into a finite number of weather types (WTs) through the use of Principal Component Analysis
251 (PCA) and a sequence of three data mining techniques: Maximum-Dissimilarity (MDA), K-
252 means (KMA) and Self-Organizing Map (SOM) algorithms. This approach was used in this
253 study in order to characterize the weather patterns that generate the wave conditions for
254 triggering headland bypassing.

255 Figure 2 illustrates the main steps of the weather typing framework for which historical data of
256 both regional SLP fields (see section 3.1.1. Atmospheric Data) and local sea-states (see section
257 3.1.2. Wave Data) are required. Then, the identification of the weather types is done in four
258 steps: i) definition of spatial domain, ii) estimation of sea level pressure and sea level pressure
259 gradient; iii) reduction of dimensionality by means of a Principal Component Analysis (PCA)
260 and iv) application of the cluster techniques to time series of PCs to define the main weather
261 types of the study area.

262 The spatial domain was defined based on the results obtained by Silva et al. (2021b). Those
263 authors applied the ESTELA methodology (Evaluating the Source and Travel-time of the wave
264 Energy reaching a Local Area - Pérez et al., 2014) to demonstrate that the primary generation
265 zone of the swell and sea that reach the study area is within both the Coral and Tasman Seas, but

it could extend over the Pacific Ocean Basin for less frequent distant swells. To ensure the use of the proper spatial domain, in this study a sensitivity test was undertaken using multiple geographic areas (see Supplementary Table 1). A multivariate linear regression model was applied using the times series of the PCs obtained from the different spatial domains as predictors (see details of the Principal Component Analysis below) and the daily average of wave parameters as predictand. The linear regression model was calibrated with data from 1987 to 2017 and validated with data from 2018 to 2020 (see Supplementary Figure 1 and 2). The optimal spatial domain was identified as the area that resulted in higher correlation in the linear regression analysis, which was the one that extends from 0 to 60°S and 140°E to 170°W.

The SLP and SLP gradient, which represents the geostrophic wind conditions (Camus et al., 2014), are obtained within the spatial domain defined in the previous step. Sea-level pressure data over land regions are not directly relevant for wave generation and is disregarded to avoid adding the variability of these areas to the analysis. According to Silva et al. (2021b), waves generated near the domain boundaries take about three days to reach the study region. This means that it can be a lag between the moment that the atmospheric condition generates the waves and the moment that the wave reaches the target point nearshore. In order to verify the relevance of the wave travel time, a multivariate linear regression model between the time series of daily principal components and wave time series considering time lags of zero to 9 days (see Supplementary Figure 3) was assessed. Higher correlation was obtained with zero to 1-day lag, indicating that a 1:1 assessment is sufficient for this study that aims to characterize the relationship between daily WTs and the wave conditions over the interest region.

The Principal Component Analysis is applied for a concatenated matrix of daily averages of SLP and SLP gradient fields. This technique allows eliminating data dependence while it reduces the dimensionality of the dataset (Camus et al., 2014). From this analysis, only the principal components that explain 95% of the variance (first 162 out of 12419 PCs for the selected domain area) are taken to the subsequent weather type classification steps. The new PC-space is then divided into a pre-defined number of clusters using the KMA algorithm. This technique groups similar data into clusters that are characterized by a prototype that represents the centroid of the group, also called weather type. KMA needs a set of initial prototypes (“seeds”) to initiate the clustering. Here, the seeds were obtained by applying the MDA algorithm that ensures the selection of the most representative and distinct data within the initial dataset (Camus et al., 2014). Every data is attributed to the cluster with the most similar prototype (Hastie et al., 2001). The centroid is recalculated and the distances between data and prototypes are calculated again to redefine the groups. The loop continues until a defined stability is achieved.

The number of clusters is variable and not statistically determined. Due to the large variability of the synoptic circulation in the study area including several distinct storm events that have been observed to be relevant for shoreline variability (e.g., Harley et al., 2022) and headland bypassing (e.g., Silva et al., 2021a), 225 clusters (WTs) were used. Synoptic charts of specific storm events – such as Tropical Cyclone Oma – were visually compared to the daily WTs to confirm if these atmospheric systems and their trajectories were being well represented. Finally, the WTs were self-organized within a bidimensional lattice (N = 225 = 15x15) using the SOM technique, which distributes the WTs along the lattice based on the similarity criterion among them to provide a more efficient visualization of the results (Camus et al., 2014).

The result is presented in Figure 3a where the WTs from WT1 to WT225 are distributed along the columns. In Figure 3b, the occurrence (total number of days) of each WT during the last 33

years (1987 to 2020) is presented, while Figure 3c shows the variability of this occurrence over seasons: austral summer (DJF), austral autumn (MAM), austral winter (JJA) and austral spring (SON). The occurrence of each WT is also calculated for ENSO and PDO periods in order to investigate if there is any influence of these climate drivers on the long-term WTs variability. Each of these WTs have generated specific wave conditions (significant wave height and peak direction) that are represented in the wave roses distributed in a 15x15 lattice according to the WTs distribution (Figure 4).

3.3. Process-based Numerical Modelling

This study uses Delft3D, a process-based numerical model to simulate the waves, currents, sediment transport and morphological variability near the headland for four events of headland bypassing (Figure 2). The model was run using coupled WAVE and FLOW modules in online mode. The wave model domain included three grids: one regular regional grid covering a region of 163 x 48 km extending from Byron Bay (northern NSW) to North Stradbroke Island (Southeast QLD) (Figure 1a) and offshore until the location of the CAWCR wave model output point with a grid resolution of 1.2 x 1.2 km; a regional curvilinear grid was nested within the regional regular grid and covers an area of approximately 150 x 20 km with grid resolution of 300 x 600 m; and a nested local curvilinear grid with a 16 x 6 km of area centered on Fingal Head and extending from Kingscliff to the south and Tweed River to the north (Figure 1b). The local wave grid resolution varies from 345 x 110 m in the outer cells to 45 x 28 m near the headland. The flow module grid is two rows smaller than the local wave grid on the offshore, south and north boundaries (Figure 1b). The topo-bathymetric data for the regional grids was obtained from the 100-resolution digital elevation model from Project3DGBR (Beaman et al., 2010) while the local wave and flow grids included the detailed topo-bathymetric survey of November 2018 from Silva et al. (2021a). All simulations were initiated with the same topo-bathymetric data which represents a spring-summer condition with an accreted beach on the updrift and no large sandbar formation.

The four selected storm events were simulated within a 45-day period with about 15-20 days to ensure initial model warm up and about 15 days after the storm event for completion of the process. The CAWCR wave hindcast was used (see section 3.1.2. Wave data) with 72 directional bins for the local wave grid, and 40 frequency bins ranging between 0.02 Hz and 1 Hz. Diffraction and refraction were activated to reproduce the wave transformation on the nearshore reefs, Cook Island and Fingal Head. The coupling interval between the FLOW and WAVE modules was set to 60 minutes. The flow model was run in 3D mode with 10 sigma vertical layers and a time step of 1 minute. The water level time series was obtained from the Tweed River tide gauge (Figure 1b) and imposed uniformly at the offshore boundary. The wind time series available from the Gold Coast Seaway Weather Station (Figure 1a) was used for the simulation. The south and north boundaries were set as Neumann for the flow conditions. Finally, morphological changes were activated within the FLOW module for the simulations.

The model was calibrated using the period from 29 November 2018 to 22 March 2019, which represented a variety of wave conditions including a major storm event (Tropical Cyclone Oma). Topo-bathymetric data was available for the beginning and end of the simulation, allowing for morphological calibration. Parameters such as wave-related suspended and bed-load transport were adjusted (both with a value of 0.3) in order to improve the sediment transport as well as horizontal eddy viscosity and diffusivity (2 and 20 m^2/s, respectively) that were used to ensure the currents deflected as they pass the headland and produce realistic morphological changes.

Modelled time series of significant wave height, peak period, direction and water level were compared to the nearshore Tweed Wave Buoy and Tweed River tide gauge measurements (Figure 1b). Time series comparisons are presented in the Supplementary Material Figure 4. Statistical results of the Root Mean Square Error (RMSE), Mean Absolute Error (MAE) and Bias were considered satisfactory (Table 1). The Brier Skill Score was used to assess the morphology simulation providing a result of 0.53, which is considered reasonable/fair according to van Rijn et al. (2003).

Table 1. Error statistics for significant wave height (Hs), peak period (Tp), direction (Dirp) and water level (WL).

	Hs	*Tp*	*Dirp*	*WL*
RMSE	0.29	1.76	23	0.01
MAE	0.20	1.30	15	0.01
BIAS	0.003	0.003	0.004	0

4 Results

First, an overall description and number of occurrences of the WTs (Figure 3) obtained is presented and related to the wave conditions that were generated by each of these atmospheric patterns (Figure 4). Then, some WTs responsible for the storm events that triggered HB over the years are distinguished (Figure 5). These storm wave events are simulated through numerical modelling (Figure 6) and the most relevant WTs for the development of the bypassing pulses are identified. Finally, the variability of these WTs is analyzed over time considering ENSO and PDO (Figure 7) phases.

4.1. Weather Types and Associated Wave Parameters

From the 225 WTs, 100 WTs account for 90% of the frequency of occurrence, with each of these WTs happening at least 50 times (days) during the period considered here. These WTs are grouped in the central part of the matrix (Figure 3b) and are primarily representing the variability of the position and intensity of the high-pressure systems (anti-cyclones) over the Tasman-Coral Sea (Figure 3a – WTs within the black line delimitation). Wave characteristics associated with these WTs show a large directional range attributed to each WT, particularly varying from east (90º) to south (180º), and with wave heights mostly lower than 2 m (Figure 4). Additionally, a few WTs within this group present a high-pressure system in combination with a strong low-pressure system developed over the Tasman Sea, such as in WTs 117 and 118 (Figure 3a). For each of these WTs, a stronger southerly wave component with wave heights reaching around 5 to 6m is observed (Figure 4).

In the outermost cells of the WTs lattice are distributed the 125 WTs that correspond to only 10% of the total frequency of occurrence (Figure 3b), which means that each one of them has occurred less than 50 days out of the 12419 days. These WTs are mostly representing the variability of strong low-pressure systems such as Tropical Cyclones that occur over the Coral and Tasman Seas (Figure 3a). While the probability of occurrence of these WTs is very low, there is a large variety of atmospheric patterns and trajectory of migration of the pressure systems among them. For instance, 91 distinct WTs have occurred less than 10 times and 33 of them happened only once. In terms of wave conditions, these less frequent WTs have a substantial contribution on the generation of easterly storm wave events with wave heights

between 2 and 4m (Figure 4). Some Tropical Cyclones, such as the ones represented by WTs 79, 94, 108 and 109, approach the coast and interact with strong high-pressure systems (Figure 3a) which can generate wave heights up to 8m varying from east-northeast to south-southeast (Figure 4).

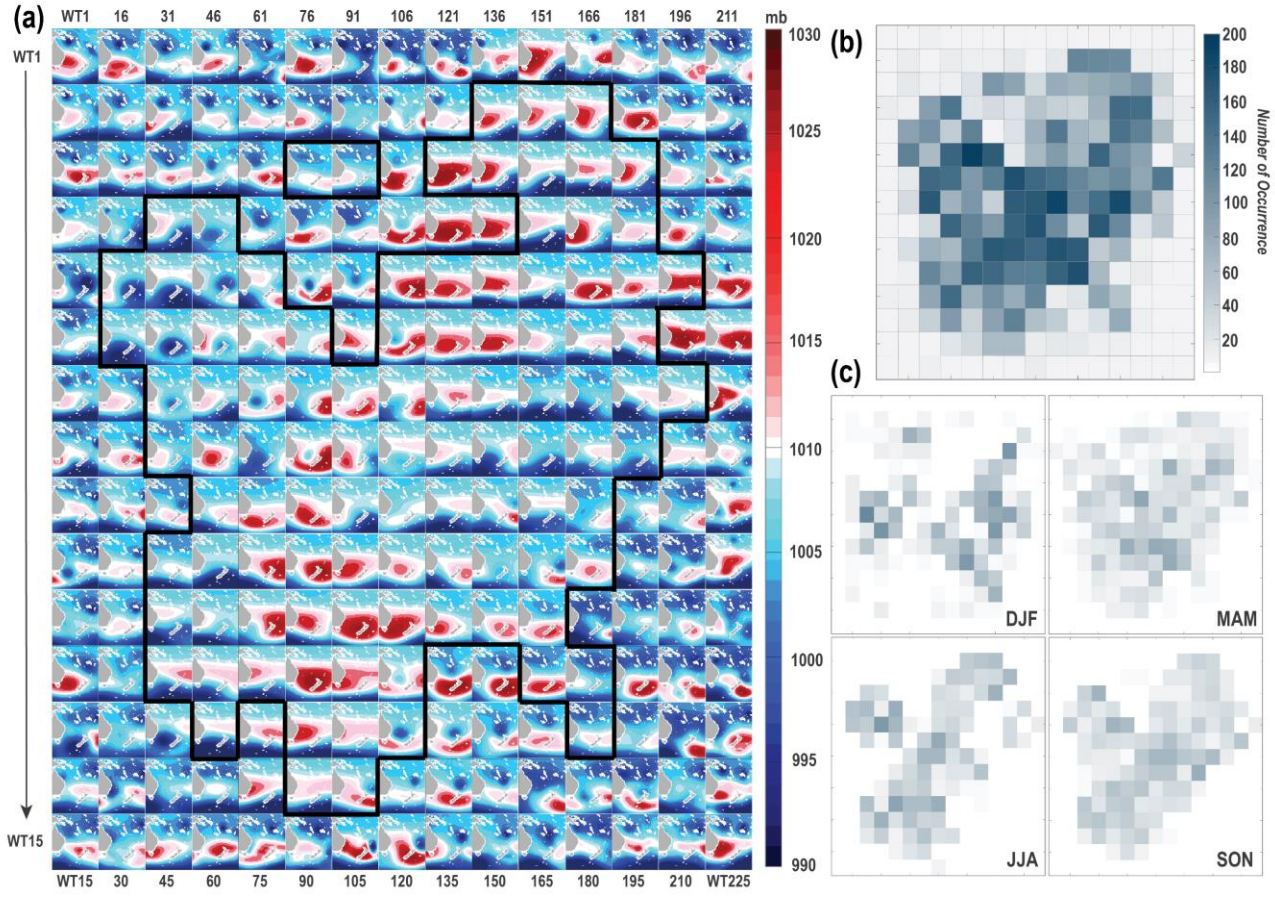

Figure 3. Weather Types (WT) lattice and number of occurrences of each WT. (a) Matrix presenting the 225 WTs distributed per column (1-15, 16-30, …, 211-225). Sea-level pressure is presented in millibars with red colors indicating high pressure and blue shades showing low pressure systems. (b) presents the number of occurrences (grey to blue scale) for each WT over the total study period. (c) Seasonal variability in the number of occurrences of each WT. DJF – austral summer, MAM – austral autumn, JJA – austral winter and SON – austral spring months. Black contour in (a) indicates the WTs that have occurred more than 50 days over the 33 years.

As for the seasonal variability (Figure 3c), austral summer (177 WTs) and autumn (183 WTs) show a large range of WTs occurring during these seasons including extreme weather events (Figure 3a). For the summer season, 26 WTs with at least 50 days of occurrence represent 60% of the atmospheric variability, while for the autumn season only 14 WTs happened at a minimum of 50 days, and this represents 29% of the frequency of occurrence for the season. The most frequent WTs over summer, such as WT 38, are characterized by less intense high-pressures (about 1010-1013 mb) located southward over the Tasman Sea (Figure 3a). During autumn, the anti-cyclone is still frequently observed southward but more intense (about 1015-1020 mb), as

414 can be observed for WTs 97 and 115. For any of these WTs, wave conditions generated vary
415 from the east to south direction with wave heights up to 3m (Figure 4).

416 Austral winter and spring have a reduced variety of WTs occurring (108 and 123 WTs,
417 respectively), which are mostly concentrated in the center of the WTs matrix (Figure 3a,c). For
418 the winter season, the most frequent WTs (23 WTs with minimum of 50 days of occurrence)
419 account for 48% of the atmospheric patterns' variability. The atmospheric patterns represented
420 are mostly extensive and strong high-pressure systems (above 1025mb), sometimes combined
421 with the intrusion of a low-pressure system near the southeast coast such as in WT 71 (Figure
422 3a). These atmospheric systems can also generate waves from east to south; however, the
423 directional range for each WT is narrower than for the events from summer (e.g., WT167 in
424 Figure 4). Finally, during spring, 15 WTs have occurred at least 50 days and represent 29% of
425 the frequency of occurrence. Among these WTs the primary characteristic is a less intense high-
426 pressure center (1010 mb) displaced towards the east (Figure 3a) with associated wave
427 conditions varying from 0 to 180º and low wave heights (e.g., WT 21, Figure 4).

428 4.2. Storm Events Triggering Headland Bypassing Pulses

429 Based on the shoreline analysis presented by Silva et al. (2021a), four headland bypassing pulses
430 that occurred recently (August-September 2014, March 2017, January 2018, and February 2019
431 indicated in Figure 2) were selected (Figure 5). Figure 5 presents the sequence of daily weather
432 types observed during each of the storm events as well as a wave rose with significant wave
433 height and peak direction for the period.

434 Storm event 1: Figure 5a shows the most recent significant HB event in Fingal Head that
435 occurred in February 2019 due to the passage of Tropical Cyclone Oma. From the 17 February,
436 TC Oma started migrating southwest from Vanuatu towards the Queensland coast in Australia
437 (Figure 5a). Until the 21 February, TC Oma's position generated waves approaching the study
438 area from the E-NE (60-90º) corresponding to about 70% of the wave direction variability of the
439 event, and with 56% of the offshore Hs ranging between 1 and 2 m and about 23% between 2
440 and 4 m. On 22 and 23 February, TC Oma reached the position represented by WT48, located
441 between 25º and 30ºS and began transitioning to a Subtropical Cyclone. During these two days,
442 the wave direction shifted to SE (130-150º) comprising 27% of the total variability from the
443 eight days period, while offshore Hs varied between 4 and 6 m, constituting about 20% of the
444 wave height distribution. Then, on the 24 February TC Oma began to dissipate whilst migrating
445 northeast.

446 Storm event 2: In January 2018, a bypassing event was triggered due to the migration of a low-
447 pressure system into the Southern Tasman Sea (WT 82 and 68 in Figure 5b). It continued
448 moving along the Southeast Australian Coast until it reached 30-35ºS and persisted in this
449 location between 14 and 16 January, represented by WTs 174 and 118. About 90% of the wave
450 direction distribution during this event occurred between S-SE (150-180º), and the highest Hs
451 values were observed on 16 January (WT 118) exceeding 5 m. The wave height, however,
452 decreased fast as the low-pressure system migrated southeast towards New Zealand (WT 37) and
453 then decayed.

454 Storm event 3: Weather type 118 and 37 were also observed in the storm event that initiated the
455 HB around Fingal in March 2017, however, the low-pressure system was initially formed over
456 the Southeast Australian Coast and then moved offshore (Figure 5c). The low-pressure system
457 persisted over the Tasman Sea (WT 118) from 6 to 10 March, generating S-SE (145-170º) waves

458 that constituted over 70% of the wave direction distribution of this event. During these four days,
459 the offshore Hs varied between 3 and 5 m which corresponds to about 50% of the wave height
460 variability. From the 11 to 15 of March, the wave height decreased, and wave direction oscillated
461 between E-SE. A low-pressure system was observed to form over the coast and moved
462 southward (WT 97) on the 13 March, but it does not consolidate (Figure 5c).

463

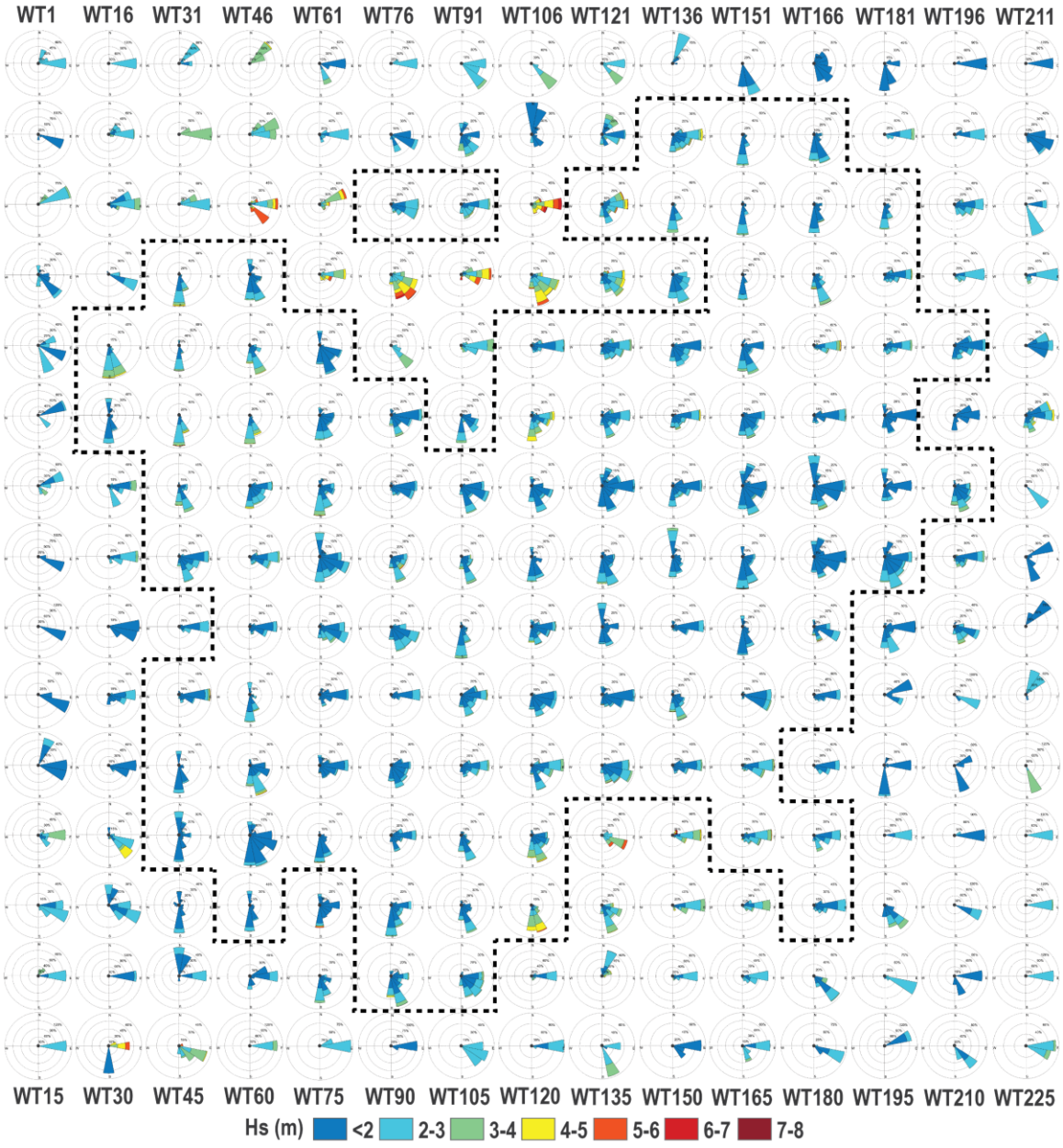

464

465 **Figure 4**. Significant wave height (meters) and peak direction (North at the top, East at the right,
466 South at the bottom, West at the left side of the wave rose) associated to each WT. Distribution
467 of wave roses along the matrix follows the WT lattice distribution. Black dashed line contours
468 the WTs that occurred 50 or more days over the 33 years.

Storm event 4: The last storm event selected occurred between August and September 2014 (Figure 5d). A low-pressure system formed at the boundary of the Coral and Tasman Seas (WT 109) and started migrating south into the central Tasman Sea to approximately 35ºS (WT 83). During the transition between WT 109 and 83 on 27-28 August, offshore Hs peaked at values between 4 and 6 m (representing 13% of the wave height variability) and SE wave direction was prevailing, ranging between 120 and 140º. The low-pressure system continued its track over the Tasman Sea and reached a location that is characterized by WT 118 (Figure 5d) between 3 and 4 September. The wave direction shifted rapidly to the south (180-200º) and Hs increased to about 4 m at this time. After that, the storm event dissipated (Figure 5d) and wave height diminished. Overall, during the full storm period, E to S-SE waves represented 70% of the wave direction variability, while wave heights were mostly (79%) between 1 and 3.5 m.

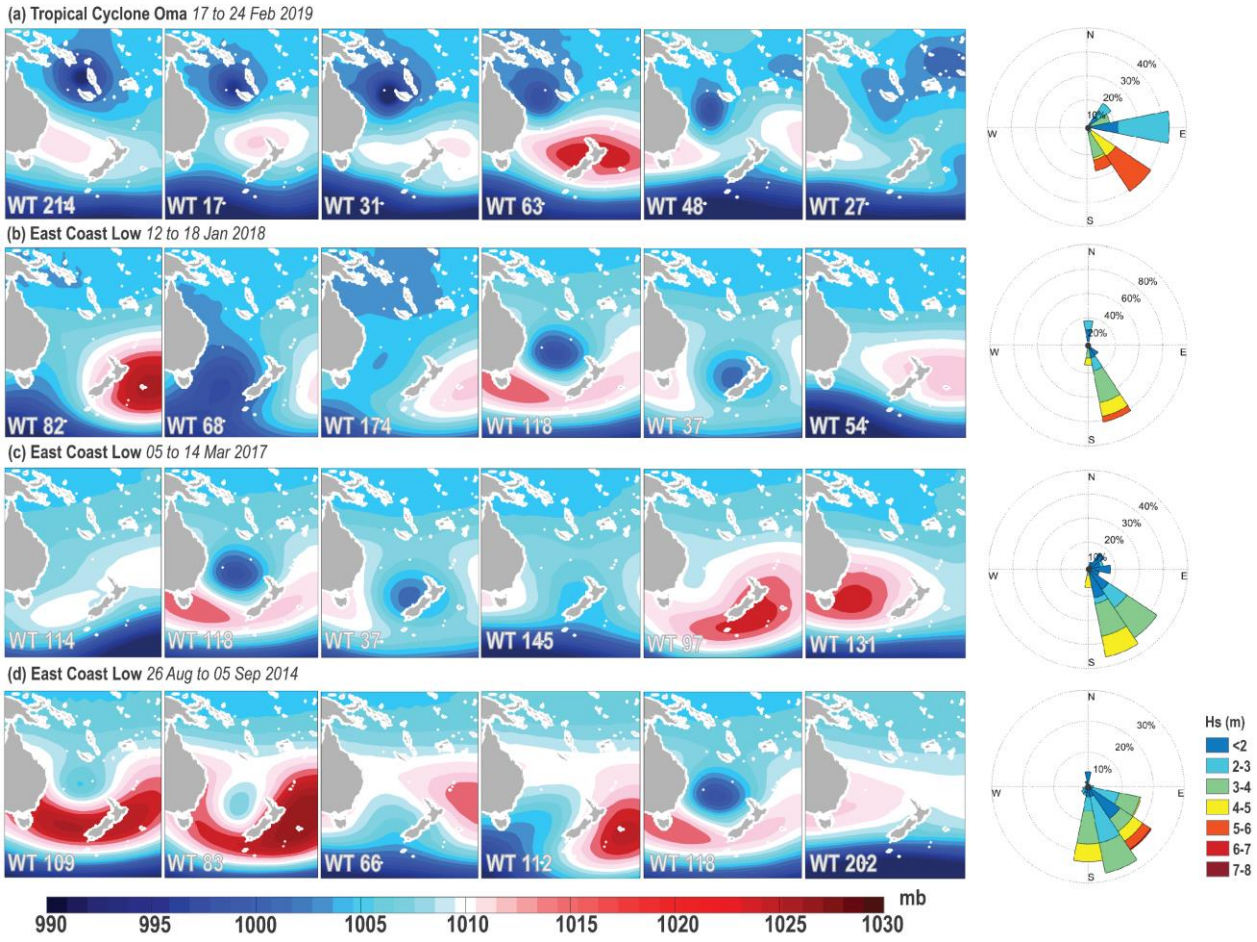

Figure 5. Four selected storm events. (a) February 2019 event (Tropical Cyclone Oma) represented during the sequence of days by WTs 214, 17, 31, 63, 48 and 27. (b) January 2018 event represented by WTs 82, 68, 174, 118, 37, and 54. (c) March 2017 event represented by WTs 114, 118, 37, 145, 97 and 131. (d) August – September 2014 event represented by WTs 109, 83, 66, 112, 118 and 202. Sea-level pressure is presented in millibars. Wave roses show the wave height (m) and direction for each storm event.

In order to understand the effect of these atmospheric patterns and associated wave conditions on the sand bypassing around Fingal Head, process-based numerical modelling was applied, and the results are presented in Figure 6 for the peak of each storm event. For TC Oma in 2019, WT 48 developed an energetic sea-state in which SE waves approached the study region with 3.5 to 5 m (Figure 6a). Wave attenuation was evident in shallower waters and a large shadow zone (Hs approximately 1 – 1.5 m) occurred to the north of Fingal Head as a result of the wave refraction and diffraction processes happening on the submerged rocky reefs and Cook Island. A strong and wide northward longshore current (over 0.8 m/s) formed within the surf-zone and increased in magnitude at the tip of the headland (Figure 6a). Also, a small recirculation cell occurred downdrift of Fingal Head, which demonstrates a process by which sediment accumulation occurs in this region (Figure 6a). The wave and current characteristics of this event led to intense sediment transport around the headland, as evidenced by the offshore sandbar (Figure 6a).

WT 118 generated high energy S-SE waves offshore in 2017 and 2018, however, both swell events showed waves approaching the study region with about half of the offshore Hs (< 2.5 m) (Figure 6b,c). These events triggered HB with a considerably weaker northward longshore current (0.3 to 0.5 m/s) compared to TC Oma 2019, although the currents intensified when passing by the headland (Figure 6b,c). The reduced sediment transport condition led to the formation of a narrower sandbar that connected to the updrift side of Fingal Head (Figure 6b,c). Then, sediment leaked around the headland and deposited on the downdrift side, where a small recirculation cell was also observed (Figure 6b,c). Interestingly, both the 2017 and 2018 storm events were followed by a second high-energy wave episode. In 2018, the second event occurred on 31 January – 1 February with offshore Hs up to 3.5 m and SE (120-140º) wave direction, which approached the coast with a Hs of about 2 - 2.5 m, influencing the formation of a northward longshore current around the headland (see results in Supplementary Material Figure 5). In 2017, the second storm event occurred on 30 to 31 March with southerly (180º) waves reaching 5.5 m offshore, but approaching the coast at about 2 m. These conditions were sufficient to form a northward longshore current that supported the sandbar migration slightly offshore and around the headland (Supplementary Material Figure 5), providing continuity to the HB process that started about 15-20 days before.

Lastly, WTs 83 and 109 generated offshore SE waves of up to 6 m, which reached the study area with Hs of about 4.5 to 5 m (Figure 6d). Similar to the other events, a shadow zone was observed in the Fingal Beach region with wave heights decreasing to about 1.5 m. This storm event generated a strong northward longshore current (> 0.8 m/s), however the current was not as wide as the currents that were formed in 2019 (Figure 6a,d). Sediment transport around the headland occurred through an offshore sandbar (Figure 6d), which was reinforced by the wave and current conditions generated during the rapid development of WT 118 a couple of days later. Finally, the small recirculation cell and sediment deposit downdrift of the headland, which were constant features of the HB in this location, are also observed in the 2014 event (Figure 6d).

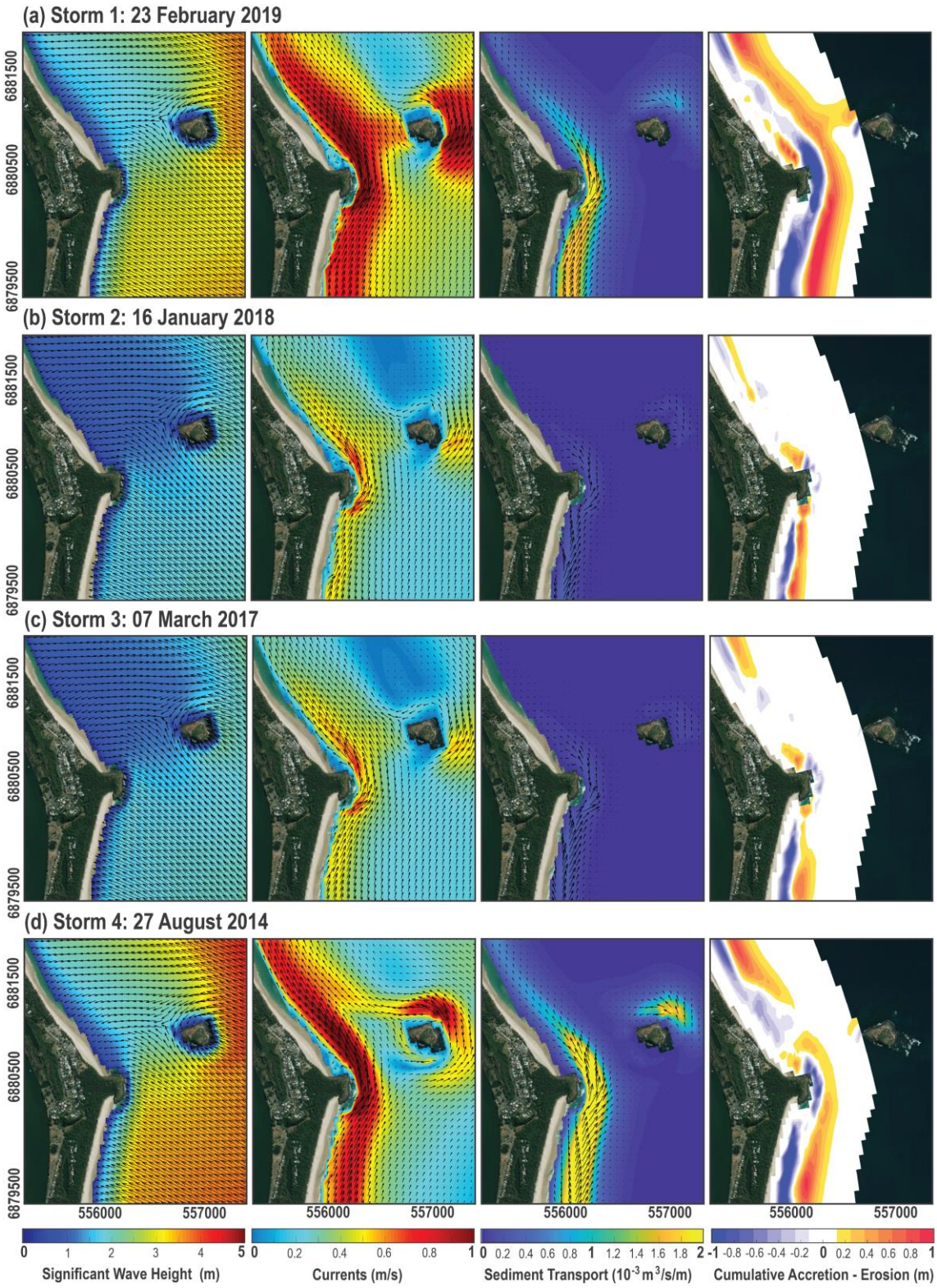

Figure 6. Waves (m), currents (m/s), sediment transport (10^{-3} m^3/s/m) and cumulative accretion and erosion (m) model results for each of the selected storm events: (a) February 2019, (b) January 2018, (c) March 2017 and (d) August-September 2014.

4.3. Weather Types Long-term Variability and Related Climate Drivers

The weather types related to storm events that have triggered recent headland bypassing (WT 48, WT 83, WT 109, 118 and WT 174) account for a total of 256 days over the 33 years of analysis (about 2 % of all the WTs variability) within 133 distinct events (single occurrences or multiple consecutive days) (Table 2). A clear seasonal distinction is observed in their occurrence with WTs 48 and 174 occurring entirely during summer and autumn months while WTs 83, 109 and 118 have about 80% of their occurrences from late autumn to early spring (April to October). Among the 133 events within the total period, 27 (23 and the four selected) events generated wave conditions similar to the storms that triggered HB (with offshore Hs > 3.5 m and primary wave direction from the S-SE). In association with these WTs, some other systems have been recurrently observed such as WT 63 (a preceding stage for WT 48), WT 67 (an ECL preceding WT 118), WT 79 (a low pressure system moving south along the QLD coast and preceding WT 109 and 174), WT 111 (an ECL formation usually related to WT 109 and 118), WT 112 (a low pressure in the Southern Tasman Sea related to WT 109 and118), WT 117 (a low pressure in the center of the Tasman Sea observed succeeding WT 83 and 118). Some other WTs as WT 20, 37, 50, 51, 98, 128 and 133 are also detected towards the end of the storm events considered here as the low-pressure systems migrate towards New Zealand.

Table 2. Weather Types related to the recent bypassing events. The table presents the total number of days that each WT occurred and the number of events it constituted. In the last column, the S-SE high energy storm events associated with the WTs are identified.

WT	*Total Days*	*Total Events*	*Identified S-SE Storm Wave Events*
48	6	5	Jan-Feb 92, Feb 19
83	35	19	Aug 89, Aug 14
109	48	34	Jun 89, Jul 89, Oct 90, Jul-Aug 93, May 96, Jul 00, May 03, Aug 06, Jun 08, Apr 09, Jul 12, Aug 14
118	54	30	Feb 99, Apr 99, Jul 99, May 05, Jul 07, Apr 09, Jul 11, Jun 12, Aug 12, Sep 14, Mar 17, Jan 18, Jul 20
174	113	45	Feb 88, Jan 18

Of these 27 storm events with potential to cause HB, about 50% (13) have occurred during ENSO (SOI index) neutral months, while the other events have been observed both during El Niño (8 events) and La Niña (6) phases. Considering just these selected events it is not possible to distinguish the influence of ENSO phases, however by evaluating the entire WT lattice (Figure 7a,b) it is noticeable that there is a distinction in the number of occurrences of each WT as a function of ENSO variability. In general, El Niño accentuates the occurrence of some WTs that are typically observed during winter and spring (Figure 3c) such as WT 71, 88, 98,100, 102, 103, 113, amongst others, that represent high pressure systems extending over a large part of the Tasman Sea and tend to be displaced northward. As a consequence, S-SE (135 to 180º) waves occur slightly more often (48%) than the E-NE to E-SE (67.5 to 135º) component (42%), and this difference increases for waves higher than 3.5 m with 73% approaching from the S-SE

(Figure 7a). Examples of WTs generating storm waves during El Niño events are WT 27, 45 and 48 (Figure 3a and Figure 4), the latter being the weather pattern identified during Tropical Cyclone Oma.

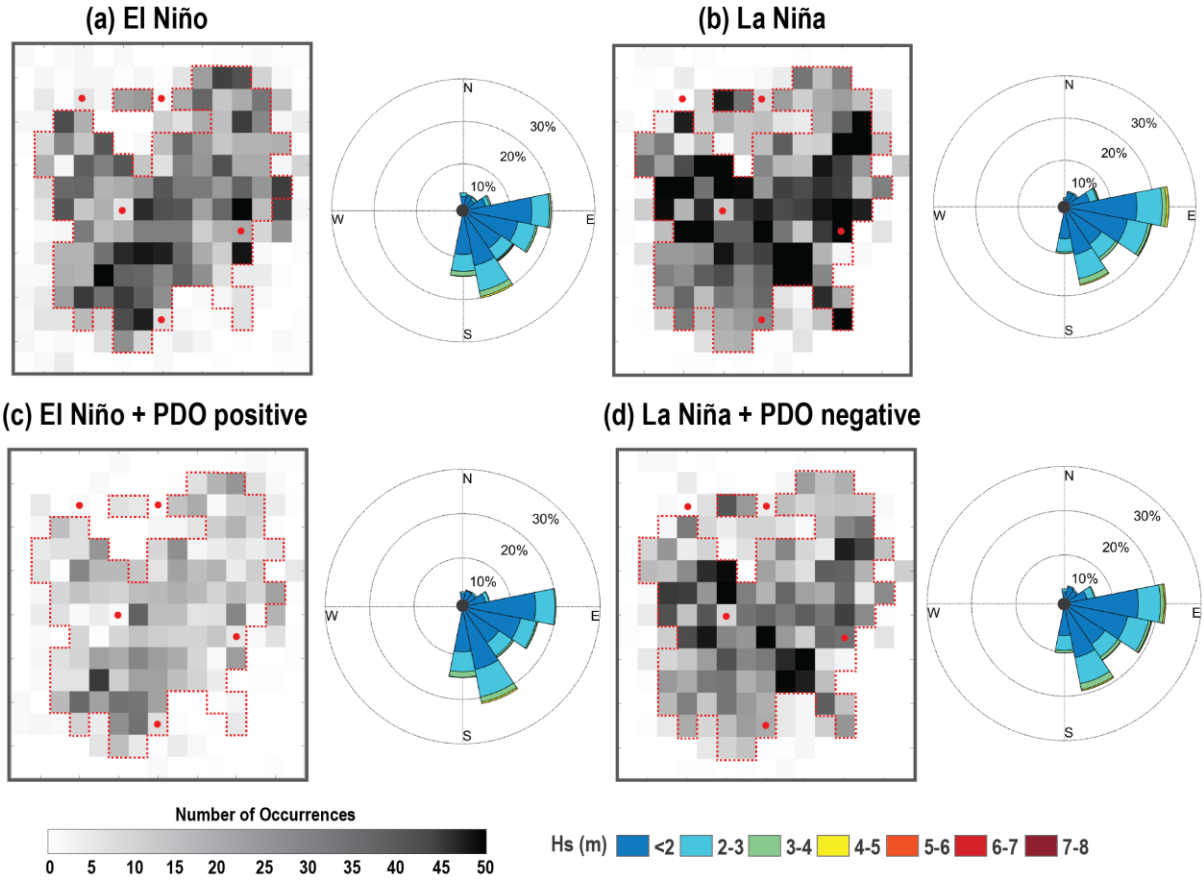

Figure 7. Number of occurrences of each weather type and the correspondent wave roses for periods of El Niño (a), La Niña (b), combined El Niño with PDO Positive (c), and La Niña with PDO negative (d). Red dashed line contours the WTs that occurred 50 or more days over the 33 years. Red dots indicate the five WTs associated with headland bypassing.

For La Niña phases (Figure 7b), the WT occurrence distribution resembles the variability for summer and autumn months (Figure 3c), such as WT 54, 69,131,170, 184, 185, among others. These WTs are characterized by a high pressure dislocated southward and frequently extending into the Pacific Ocean (Figure 3a, e.g., WT 185). Due to these characteristics, the easterly wave component (E-NE to E-SE) contributes 51% of the total variability while S-SE waves represent 42% (Figure 7b). In relation to waves with higher Hs (> 3.5 m), 59% correspond to waves from the E-NE to E-SE and 41% from the S-SE, which is not as discrepant as observed for El Niño periods. Some of the WTs generating storm waves during La Niña phases are WT 63, 64 and 94 (with over 50% of their occurrences during La Niña) representing intense low pressures moving south in the Coral Sea (Figure 3a) and producing severe storm waves (Hs >5 m) from a more easterly direction (Figure 4).

The Pacific Decadal Oscillation (PDO) is considered a long-lived ENSO phase (Johnson et al., 2020) and it has been observed to oscillate in synchronicity with long periods of accretion and erosion on the beaches adjacent to Fingal Head, in particular when co-incident with ENSO periods (Silva et al., 2021a). Results for the number of occurrences with respect to PDO cycles were similar to the observed variability during ENSO phases. To verify if a co-existence of these climate drivers could potentialize the occurrence of some atmospheric patterns, the WTs occurring during both PDO positive (negative) and El Niño (La Niña) were identified (Figure 7c,d). For PDO positive combined with El Niño phases, WTs 71, 98, 100 and 102 were most representative (Figure 3a). The general wave condition was observed to be similar to the El Niño only phases, but the percentage of waves with Hs > 3.5 m increased to about 95% from the S-SE direction (Figure 7c). On the other hand, for the PDO negative phase and La Niña combination the WTs with a greater number of occurrences are WT114, 131 and 145 (Figure 3a). The atmospheric patterns occurring during these periods generate storm waves with an equal percentage (50%) for both E-SE (90 – 135º) and S-SE (160 – 180º) directions (Figure 7d).

5 Discussion

5.1. The Headland Bypassing Mechanism around Fingal Head

Some studies have used process-based numerical modelling to investigate headland bypassing in idealized scenarios (Ab Razak, 2015; George et al., 2019) or real-life headlands (Vieira da Silva et al., 2016b, 2017, 2018a, 2021; Valiente et al., 2019, 2020; King et al., 2021) with the primary focus of isolating specific parameters and understanding their influence on the HB process. Overall, modelling sediment transport around a headland has been a challenging task (Klein et al., 2020), and especially if the purpose is to develop morphological simulations. In this sense, this study has contributed a first step into deriving through modelling the morphological changes that occur when a bypassing pulse is triggered. More importantly, these results show that the distinct bypassing pulses proposed by Silva et al. (2021a) can be initiated with marginally different storm wave characteristics.

George et al. (2019), for instance, developed a numerical model of sediment transport using idealized scenarios in order to categorize some controlling factors of the HB mechanism. The analysis showed that large and oblique waves generated more transport than smaller and oblique waves or large waves at a shore-normal angle (George et al., 2019). The present study corroborates George et al. (2019) findings showing that large waves (offshore Hs of around 6 m and Tp of 10-11 s), at the peak of the storms (2014 and 2019 events) and in an oblique direction to the coast (SE, around 130 to 140º) reached the headland with 2.5 m Hs and a direction of 110 to 120º, which resulted in strong northward longshore currents (of about 1 m/s), high suspended sediment transport (of about 4 – 5 x10-3 m3/s/m) and bed load transport (of about 10 x10-5 m3/s/m). On the other hand, the results for the storm events in 2017 and 2018 showed also that high offshore waves (with Hs of about 5 m and Tp of 13 s) but from a more southerly direction (160-165º) reached the headland with 1.5 m Hs and 110 to 120º angle. The wave height attenuation impacted on the intensity of the longshore current (of about 0.3 – 0.4 m/s), the suspended sediment transport (of about 3.5 – 6 x10-5 m3/s/m) and the bed load transport (of about 20 x10-6 m3/s/m).

More interestingly, the high energy storm events from the SE presented similar values of bed load and suspended transport at all observation points (updrift, in front of the headland and downdrift; see Figure 1), while the storm events from the south (Figure 6b,c) presented bed load

and suspended transport of one order of magnitude higher on the downdrift compared to the headland and updrift points. This suggests that the wave attenuation changed the category of bypassing (George et al., 2019; Klein et al., 2020) from an unconstrained bypassing – where there is virtually no difference between downdrift and updrift sediment transport – to a bed eroded bypassing when the sediment transport is larger around the downdrift shoulder of the headland implying the occurrence of erosion in front of the headland (Figure 6). Considering the proposed bypassing concept around Fingal Head (Silva et al., 2021a) and the present findings, the sandbar bypassing is clearly represented by two modes: the 2014 and 2019 storms showed an unconstrained sediment flux through the wide surf-zone and the 2017 and 2018 storms presented a leaking bypassing process which pushes the sediment deposited at the tip of the headland towards the downdrift beach.

A final consideration in terms of the HB mechanism is the difference of the directional range of the selected storm events. While the 2014 and 2019 storms (Figure 5a,d and Figure 6a,d) have a broader distribution of wave directions during the storm event, the 2017 and 2018 storms (Figure 5b,c and Figure 6b,c) have 70 to 90% of the waves during the storm event from the S-SE directional range. The sequencing of wave direction influencing a HB process has been observed before in multiple locations (Vieira da Silva et al., 2018a; Wishaw et al., 2021), but focused on the full completion of the bypassing pulse. Here, it was observed that there is a potential relevance of the variability of wave direction during a storm event influencing the type and magnitude of the HB pulse. The hypothesis is that the easterly wave component preceding the peak of the storm mobilizes sediment offshore and the oblique SE waves promote the downdrift movement as evidenced by the extension of the sandbar. However, to confirm this theory, a more focused study on modelling the HB process and evaluating the evolution of the storm events is needed.

5.2. Weather Types inducing Headland Bypassing

The weather types obtained in this study and their temporal variability are in general agreement with the atmospheric patterns previously described for the Tasman-Coral Seas region (Drosdowsky, 2005; Chand et al., 2019; Dowdy et al., 2019). Overall, the anticyclonic high-pressure (or subtropical ridge) dominates the spatial distribution of the SLP fields (e.g., Figure 3), particularly influencing their seasonal variability. Extensive latitudinal migrations and changes in intensity are observed for the anti-cyclones throughout the year with the most southward (northward) position and less (more) intensity of its center during summer (winter) (Drosdowsky, 2005). This latitudinal displacement of the high-pressure systems influences the wave generation zones in the study region and produces a more easterly (southerly) mean wave direction during summer (winter) months (Shand et al., 2010; Mortlock and Goodwin, 2015; Silva et al., 2021b). Autumn months showed the largest variability of WTs which results from the transitioning position of the anti-cyclone (Drosdowsky, 2005) allowing the migration of Tropical Cyclones to the south and the low-pressure systems (e.g. ECLs) along the coast to the north. Within this condition, wave generation occurs over a wider area of the Coral-Tasman Sea (Silva et al., 2021b) and with higher waves, on average, reaching the study region (Shand et al., 2010).

The WTs also well-represent the large variety of extreme events (Figure 3) that are formed over the Coral-Tasman Sea, in agreement with previous studies (Rueda, 2013; Chand et al., 2019; Dowdy et al., 2019). Among these atmospheric patterns, strong low-pressure systems that are positioned near the coast between 25 and 35ºS (mid-latitudes) have the potential to generate

headland bypassing around Fingal Head. These events can be originated from Tropical Cyclones that migrate south, becoming a post-tropical cyclone (Dowdy et al., 2019). The southward TC tracks are less frequent than TC tracks over the northern part of the Coral Sea (Chand et al., 2019), but have happened a few times in the past (Gray et al., 2020). For instance, in the summer of 1992, two successive TCs (TC Betsy 6-13 January and TC Daman 15-18 February) moved south along the Queensland coast approaching a position represented by WT48 (similar to TC Oma). Both events presented waves from the E to S-SE which reached 3.5 to 4.5 m Hs, leading to a HB pulse at Fingal Head according to the shoreline dataset from Silva et al. (2021a). In March 1993, TC Roger triggered headland bypassing while it migrated from the Solomon Islands towards 25ºS near Fraser Island (QLD). The WTs associated with this 10-day event follow the sequence of WT 198, 63, 108, 131, 99 (Figure 3a). All of them present a range of incident wave direction from the E-NE to S-SE, with the peak of the storm (Hs of up to 6 m) having wave direction of about 90-100º followed by several days with waves over 1.5 m from the S-SE. In March 1995, TC Violet (represented by WTs 79 and 174) generated SE waves of up to 5 m of Hs while migrating southward along the coast to about 30ºS, which led to another bypassing pulse. In March 2004, TC Grace (characterised by WTs 94 and 64) moved south along the coast and underwent extratropical transition, generating waves from the E-SE of about 2 to 4 m, triggering a pulse of headland bypassing at Fingal Head.

On the other hand, severe TCs that crossed the coast in Southeast Queensland and Northern NSW such as TC Nancy (Jan-Feb 1990) and TC Oswald (Jan 2013) (Gray et al., 2020) did not trigger a bypassing pulse as these low-pressure systems moved too close or over the coast producing high energy E-NE waves. TC Debbie in March 2017 was also a remarkable coastal-crossing TC, causing landfall over Brisbane (QLD) region. However, different from the above mentioned TCs, TC Debbie actually moved back offshore as a strong low-pressure system and reinforced the already triggered bypassing of early March 2017 (Figure 5c and Figure 6c). Note that weather type clusters do not represent the transformation of these TCs over land as sea-level pressure variability over the continents was neglected from the principal component analysis.

East Coast Lows are another class of intense low-pressure systems that can occur near the mid-latitudes offshore the East Australian coast (Dowdy et al., 2019). These atmospheric systems are very diverse in terms of cyclogenesis, structure and temporal variability (Browning and Goodwin, 2013; Dowdy et al., 2019). WTs 67, 80, 83, 109, 111, 117, 118 and 174 represent some of the more common examples of these atmospheric patterns. Silva et al. (2021a) suggested some potential bypassing events based on the sandbar position offshore, from which nine were related to ECLs generating S-SE (150 to 180º) storm waves higher than 3.5 m, such as Feb 1988 (WT174), June 1989 (WTs 109, 111 and 117), October 1990 (WTs 109, 111), March 1998 (WTs 108 and 111), July 1999 (WTs 111and 118), May 2003 (WT 109), May 2005 (WTs 111, 117, 118), July 2011 (WTs 67 and 118), July-Aug 2012 (WTs 109 and 118). Among these events, the most common WTs were 109, 111, 117 and 118 that represent a low pressure centered at 30 to 35ºS with associated strong high-pressure systems to the south. Additionally, the storms mentioned above were reasonably long-lived events with some lasting for over a week, whereas ECLs are known for being explosive systems that intensify rapidly and last only for few days (Dowdy et al., 2019). Finally, as for the Tropical Cyclones, some ECL events are well-known for causing high wind damage, intense erosion, and flooding in coastal cities which may not necessarily be related to headland bypassing. For example, the June 2016 ECL represented by WTs 111 and 67 produced E-NE storm waves that led to severe erosion of Southeastern Australia beaches (Harley et al., 2017), but it was not as significant for the Northern NSW region

719 including Dreamtime and Fingal beaches due to the limited fetch of the wind-generated waves in
720 the north of the region.

721 In total 19 storm events are presented here that were related to shoreline and/or sandbar changes
722 in the study region concurrent with some of the relevant WTs identified over the 33-year period.
723 Although it is expected that these are not the only events that have triggered HB or had the
724 potential to produce a sand pulse at Fingal Head (e.g., Table 1), they have provided some
725 distinguishable characteristics that support the development of an understanding of how
726 bypassing events were initiated in the past and what they had in common. Overall, the few TCs
727 leading to HB occurred between February and March and during the accretionary periods in the
728 study area (1992 to 1996, 2004 to 2007 and 2014 to 2020) (Silva et al., 2021a). Conversely, the
729 ECLs inducing bypassing listed above occurred mainly between May and July and coincided
730 with the periods where the updrift beach was eroded (1988 to 1990, 1997 to 2003, and 2009 to
731 2013) (Silva et al., 2021a). This implies that the atmospheric patterns related to HB at Fingal
732 Head could occur anytime. However, it also suggests that TC-related bypassing requires more
733 sediment availability and likely leads to larger volumes of sand transported such as during TC
734 Oma (Figure 6a); whereas the ECLs can produce HB pulses with lower volumes of sand being
735 transported around the headland such as the events in 2017 and 2018 (Figure 6b,c).

736 Lastly, the WTs identified to be pertinent for HB did not show evident links to ENSO and PDO
737 phases. Studies of TC genesis and frequency for the Coral Sea and Southwest Pacific have
738 shown that La Niña phases tend to have an above-average number of TCs per season
739 approaching the far south of the Queensland coast (Chand et al., 2019). This occurs as a function
740 of a displacement of the South Pacific Convergence Zone (SPCZ) towards the southwest
741 influencing the dislocation of the cyclogenetic regions (Brown et al., 2020). However, from the
742 few TC events observed migrating south and identified as generating bypassing, three were
743 during strong El Niño months and two during transition to La Niña, which does not suggest any
744 obvious connection with these climate drivers. In fact, for this number of events, it is not
745 statistically possible to develop any relationship. The same applies to ECL events which are
746 already described in the literature as having only discrete connections to ENSO phases (Dowdy
747 et al., 2019) with a potential increase in occurrence during transitioning periods between strong
748 El Niño to strong La Niña (Hopkins and Holland,1997). Altogether, it might not be possible to
749 distinguish the climate driver that specifically induces the occurrence of the WTs that have
750 triggered bypassing, but a distinct long-term variability of the shoreline position near Fingal
751 Head exists and it is correspondent to multiannual to decadal cycles of ENSO and PDO (Silva et
752 al., 2021a). Hence, it is likely that the cyclicity of headland bypassing around Fingal Head is
753 driven by the long-term sediment availability updrift.

754 Klein et al. (2020) stated that sediment availability is a key factor for the HB process as it
755 influences the net long-term magnitude of the sand pulse. However, sediment accumulation
756 updrift of the headland is dependent on a persistent oblique wave climate intensifying the
757 longshore sediment transport (Ribeiro, 2017). In the present study, it was observed that El Niño
758 and the PDO positive phase reinforce the winter-like WTs and southerly wave component, while
759 La Niña and the PDO negative phase present the opposite pattern with more WT characteristics
760 of the typical summer-autumn period. These conditions are expected to have a substantial
761 influence on the northward longshore transport (Splinter et al., 2012) and therefore explain the
762 shoreline variability observed by Silva et al. (2021a) – i.e. positive (negative) PDO phases and

long periods of El Niño (La Niña) corresponding to a more accreted (eroded) upper beach updrift of Fingal Head.

5.3. Potential for Headland Bypassing under Climate Projections

Climate change is altering the atmospheric circulation, the teleconnection patterns, and consequently, the wave climate (Hemer et al., 2013; Reguero et al., 2019). For the Eastern Australia Coast, predictions of latitudinal changes of the subtropical ridge (Drosdowsky 2005; Grose et al., 2015), displacements of the SPCZ (Brown et al., 2020), and variability of the tropical and extratropical cyclones frequencies (Dowdy et al., 2013; Chand et al., 2019; Speer et al., 2021) have been alarming for the impacts and associated uncertainties on wave power (Odériz et al., 2021), wave direction (Lobeto et al., 2021), sediment transport (Vieira da Silva et al., 2021; Zarifsanayei et al., 2022), and ultimately, the local coastal processes and shoreline.

The findings from this study showed that Tropical Cyclones and East Coast Lows are necessary to trigger a bypassing pulse in Fingal Head, although the headland may "leak" sand under modal wave conditions if the updrift beach is fully accreted (Silva et al., 2021a). Projections for TC activity in the East Australia region indicate a trend towards fewer cyclones in particular over the peak season (Dowdy, 2014; Chand et al., 2019). On the other hand, several studies have suggested a poleward migration of the TC genesis and location of maximum intensity (Kossin et al., 2014; Daloz and Camargo, 2018; Shan and Yu, 2020), which result from the tropical expansion (Yang et al., 2020). If the updrift beach has enough sediment supply, fewer and southerly dislocated TC tracks, as predicted, could potentialize HB at Fingal Head, such as during the TC Oma event where one TC triggered a large bypassing pulse during that season. On the contrary, if TC occurrences increase, it could enhance upper beach erosion and not facilitate the bypassing pulse completion which requires less energetic sea states (Wishaw et al., 2020; Silva et al., 2021a). Another variable for the future scenarios is the proximity of the cyclones to the coast during the TC migration, since it was observed that TCs that crossed the coast were not efficient in developing sand bypassing at Fingal Head.

For the ECLs, trends and future projections are unclear as these systems have large spatial and temporal variability which leads to inconsistencies in the historical records (Dowdy et al., 2019). Dowdy et al. (2013) suggested that a decrease in the number of winter ECLs could occur along the east coast of Australia from around 20 to 30°S. Speer et al. (2021) found that thee ECLs had a maximum intensity near 28°S during 1970-1994, but this pattern has moved south to about 34°S, 153°E since 1995. Overall, the uncertainties in ECL trends make it difficult to provide any estimate of how they would impact the coastal processes. However, if these systems are being dislocated to higher latitudes, it is likely that a reduction in HB pulses triggered by ECLs would occur, as for the example of WT 67 that characterises the June 2016 ECL that led to erosion but no significant bypassing.

In addition to the expected variations to the regional atmospheric patterns, the global-scale climate drivers that have been related to long-term sediment availability for the bypassing pulses (Silva et al., 2021a) are also subject to future changes. Over the last 50 years ENSO extremes have been significantly stronger (Grothe et al., 2020) and a recent study showed that El Niño events might develop faster and persist over longer periods (Lopez et al., 2022). These projections could indicate a potential for longer periods of sediment availability updrift of Fingal Head. At the same time, models have shown an increase in strong El Niño to La Niña transitions (Chen et al., 2017; Lopez et al., 2022) and overall wave projections have suggested that a more

La Niña-like mean state would dominate the wave climate in Eastern Australia (Hemer et al., 2013). In that case, erosive periods would also be intensified at Dreamtime Beach. Finally, PDO predictability has been suggested to reduce under a warming climate (Li et al., 2020), which does not satisfy any potential prediction of future changes in sediment availability due to this driver.

In summary, considering all uncertainties associated with the trends and projections of atmospheric patterns and climate indices discussed, linear trends towards either more or less bypassing are not likely to occur within the scope of current climate projections. In fact, it could be expected that the cyclicity of the HB process will be maintained but the magnitude will be intensified, as a consequence of the potential for more extreme ENSO phases and the spatial variability of the relevant atmospheric systems. In other words, the periodic accretion resulting from longer lasting El Niño's can provide sediment for larger bypassing pulses under the influence of the southward position of TCs, whereas the transition to strong La Niña phases can lead to dramatic subsequent erosive periods. Altogether, putting this in the context of the challenges for shoreline predictions (Splinter and Coco, 2021), it becomes evident that climate projections cannot be translated linearly to local coastal processes. While global-scale wave forecasting based on climate scenarios can be linked to general shoreline trends, this knowledge needs to be much more refined in order to reproduce the complexity of local scale coastal processes and better inform coastal management decision-making.

6 Conclusions

Using weather type clustering techniques and process-based numerical modelling, this study identified the synoptic systems that have generated the ideal wave conditions to trigger bypassing pulses around Fingal Head (New South Wales, Australia). Overall, results showed that the occurrence of the specific weather types could support different bypassing mechanisms, but it is the long-term sediment availability that controls the multiannual to decadal cycles of headland bypassing. Furthermore, this study aimed at disentangling the relationship between large-scale climate drivers, atmospheric systems, waves and a local coastal process, which effectively highlighted the complexity of conceptualizing headland bypassing and predicting its occurrence.

Tropical Cyclones and East Coast Lows approaching mid-latitudes (30°S) are necessary to initially develop a bypassing pulse in the study area. However, not every TC or ECL migrating towards this zone is able to trigger a HB episode. Some potential influences include the trajectory of these atmospheric systems as it was observed that severe TCs crossing over the coast can lead to massive erosion but no substantial bypassing; persistence of a TC in a particular location which can influence the formation of the appropriate wind fetch for wave generation; and sediment availability on the updrift side of the headland that limits the magnitude of the pulse. Considering all these characteristics, Tropical Cyclone Oma (February 2019) was the precise example of a weather type capable of triggering a large sandbar bypassing event.

This study also provides, for the first time, morphological simulations of real-life bypassing pulses. The four selected storm events presented two distinct headland bypassing mechanisms, in agreement with previous literature. The sandbar bypassing mechanism was observed to be a larger sand pulse with an unconstrained characteristic of the sediment transport while the sediment leaking mechanism showed stronger sediment transport on the downdrift compared to the updrift, leading to erosion at the tip of the headland. The offshore waves forcing the models varied from 5-6 m Hs and around 130° wave direction for the sandbar bypassing while for the sand leaking pulse wave heights were 4-5 m and from 160°. All storms reached the study region

with SE (110-120°) wave directions, but the more southerly storms had smaller wave heights. In this sense, wave attenuation ultimately led to the distinction between the two bypassing types.

Considering the variability of occurrence of the WTs associated with the bypassing events, no trend or significant relation was observed with the selected climate indices (ENSO and PDO). On the other hand, the overall WT lattice showed changes in the number of occurrences of weather types for the distinct phases of these drivers. Positive (negative) PDO phases and El Niño (La Niña) showed a more winter-like (summer-like) atmospheric variability with the high-pressure displaced northward (southward) and, as a consequence, storm wave directions were more common from S-SE (E-SE). Overall, this indicates that positive PDO and El Niño phases have the potential to intensify the longshore transport and provide accretion at Fingal Head's updrift upper beach (Dreamtime Beach), and vice-versa for negative PDO and La Niña events. Therefore, climate drivers are capable of influencing the long-term sediment availability and the low-frequency headland bypassing cycles.

Acknowledgments

The authors acknowledge the funding for the topo-bathymetric data collection provided by the Tweed Sand Bypassing (TSB), NSW Department of Planning, Industry & Environment and QLD Department of Environment and Science. In addition, the authors thank the Centre for Australian Weather and Climate Research (CAWCR), a partnership between the Bureau of Meteorology and CSIRO, for publicly providing this collection of 42 years of wave hindcast data. For providing access to the weather typing methodology, the authors acknowledge Prof. Fernando Mendez from University of Cantabria. Finally, Ana Paula da Silva acknowledges the financial support from Griffith University through the Griffith University International Postgraduate Research Scholarship (GUIPRS) and Griffith University Postgraduate Research Scholarship (GUPRS).

Open Research

The datasets used in this research are available via their original repositories. The weather type analysis is based on the CFSR dataset available at https://rda.ucar.edu/datasets/ds093.1/ (1987 to 2011) and https://rda.ucar.edu/datasets/ds094.1/ (2012 to 2021). Wave parameters analyzed in this study are available from CAWCR repository (https://data.csiro.au/collection/csiro:39819). Tide series is available at the QLD Government repository (https://www.qld.gov.au/environment/coasts-waterways/beach/tide-sites) and the wind series is available at the Bureau of Meteorology – BOM AUS – repository (http://www.bom.gov.au/climate/dwo/IDCJDW4050.latest.shtml). Regional bathymetry from the Project 3DGBR is freely available at https://portal.ga.gov.au/persona/marine. Local bathymetry is available per request and approval by the Tweed Sand Bypassing (TSB), NSW Department of Planning, Industry & Environment and QLD Department of Environment and Science. Weather typing codes are of intellectual property of University of Cantabria (Camus et al., 2014) and are being made available through the TESLA-Kit project (https://github.com/teslakit/teslakit).

References

Ab Razak, M.S., 2015. Natural Headland Sand Bypassing: Towards Identifying and Modelling the Mechanisms and Processes. Ph.D. Thesis, Delft University of Technology, Delft. CRC Press/Balkema, The Netherlands. (204p) ISBN 9781138028647.

Allen, M., Andrews, M., 1997. Assessment of directional wave climate variability for a sand bypassing project. In: Proceedings of Pacific Coasts and Ports '97, Proceedings of the 13th Australasian Coastal and Ocean Engineering Conference and the 6th Australasian Port and Harbour Conference, vol. Volume 2. Centre for Advanced Engineering, University of Canterbury, Christchurch, New Zealand, p. 903–908 (ISBN: 0908993161).

Anderson, D., Ruggiero, P., Antolínez, J.A.A., Méndez, F.J., & Allan, J., 2018. A climate index optimized for longshore sediment transport reveals interannual and multidecadal littoral cell rotations. Journal of Geophysical Research: Earth Surface, 123, p. 1958–1981. https://doi.org/10.1029/2018JF004689

Barnard, P.L., et al., 2015. Coastal vulnerability across the Pacific dominated by El Niño/Southern Oscillation. Nature Geoscience, 8, p. 801–808. doi:10.1038/NGEO2539.

Beaman, R.J., 2010. Project 3DGBR: A high-resolution depth model for the Great Barrier Reef and Coral Sea. Marine and Tropical Sciences Research Facility (MTSRF) Project 2.5i.1a Final Report, MTSRF, Cairns, Australia, p. 13 plus Appendix 1. Available at: http://www.deepreef.org/images/stories/publications/reports/Project3DGBRFinal_RRRC2010.pdf

Brown, J.R., Lengaigne, M., Linther, B.R., Widlansky, M.J., van der Wiel, K., Dutheil, C., Linsley, B., K., Matthews, A.J., Renwick, J., 2020. South Pacific Convergence Zone dynamics, variability and impacts in a changing climate. Nature Reviews: Earth & Environment, p. 1-14, https://doi.org/10.1038/s43017-020-0078-2.

Browning, S.A. and Goodwin, I.D., 2013. Large-scale influences on the evolution of winter subtropical maritime cyclones affecting Australia's East Coast. Monthly Weather Review, 141, p.2416-2431.

Caires, S., Swail, V. L., and Wang, X. L., 2006. Projection and analysis of extreme wave climate. Journal of Climate, 19, p.5581–5605.

Camus, P., Menendez, M., Mendez, F. J., Izaguirre, C., Espejo, A., Canovas, V., Perez, J., Rueda, A., Losada, I. J. and Medina, R., 2014, A weather-type statistical downscaling framework for ocean wave climate. Journal of Geophysical Research Oceans, 119, doi:10.1002/2014JC010141.

Cascalho, J., Duarte, J., Taborda, R., Silva, A., Bosnic, I., Carapuco, M., Lira, C., Rodrigues, A., 2014. Sediment textural selection during sub-aerial headland bypassing – An example from the Nazare coastal system (Portugal). In: Proceedings of the 3as Jornadas de Engenharia Hidrografica (Lisbon, Portugal), p.297-300 (ISBN - 978-989-705-073-2).

Castelle, B., Marieu, V., Bujan, S., Splinter, K.D., Robinet, A., Sénéchal, N., Ferreira, S., 2015. Impact of the winter 2013–2014 series of severe Western Europe storms on a double-barred sandy coast: Beach and dune erosion and megacusp embayments. Geomorphology, 238, p. 135-148.

Chand, S., Dowdy, A.J., Ramsay, H.A., Walsh, K.J.E., Tory, K.J., Power, S.B., Bell, S.S., Lavender, S.L., Ye, H., Kuleshov, Y., 2019. Review of tropical cyclones in the Australian region: Climatology, variability, predictability, and trends. WIREs Climate Change, 10, e602.

Chapman, D.M., 1981. Coastal Erosion and the Sediment Budget, with Special Reference to the Gold Coast, Australia. Coastal Engineering, 4, p.207-227.

Chen, C., Cane, M.A., Wittenberg, A.T., Chen, D., 2017. ENSO in the CMIP5 Simulations: Life Cycles, Diversity, and Responses to Climate Change. American Meteorological Society, p.775-801, doi: 10.1175/JCLI-D-15-0901.1.

Costa, W.L.L., Silveira, L.F., Klein, A.H.F. 2019. Influence of wave climate and tidal regime on headland bypassing – Study Case: Northern Sao Francisco do Sul Island, SC, Brazil. In: Proceedings of 9th International Conference in the Coastal Sediments - Coastal Sediments 2019 (Tampa/ St. Pete, Florida), p.1-14.

Costa, W., Idier, D., Rohmer, J., Menendez, M., Camus, P., 2020. Statistical Prediction of Extreme Storm Surges Based on a Fully Supervised Weather-Type Downscaling Model. Journal of Marine Science and Engineering, 8, 1028, doi:10.3390/jmse8121028.

Daloz, A.S. and Camargo, S.J., 2018. Is the poleward migration of tropical cyclone maximum intensity associated with a poleward migration of tropical cyclone genesis?. Climate Dynamics, 50, p. 705–715.

Dowdy, A.J., Mills, G.A., Timbal, B., Wang, Y., 2013. Changes in the Risk of Extratropical Cyclones in Eastern Australia. American Meteorological Society, p. 1403-1417, doi: 10.1175/JCLI-D-12-00192.1.

Dowdy, A.J., 2014. Long-term changes in Australian tropical cyclone numbers. Atmospheric Science Letters, 15, p. 292–298.

Dowdy, A.J. Pepler, A., Di Luca, A., Cavicchia, L., Mills, G., Evans, J.P., Louis, S., McInnes, K.L., Walsh, K., 2019. Review of Australian east coast low pressure systems and associated extremes. Climate Dynamics, 53, p. 4887–4910.

Drosdowsky, W., 2005. The latitude of the Subtropical Ridge over Eastern Australia: The L index revisited. International Journal of Climatology, 25, p. 1291–1299.

Durrant, T., Hemer, M., Smith, G., Trenham, C. and Greenslade, D., 2019. CAWCR Wave Hindcast - Aggregated Collection. Volume 5, CSIRO, Service Collection. 102.100.100/137152

Fox, I., 2016. The Fragile Edge: A Natural History of the Tweed Coast. Fragile Edge Publishers, 450p., ISBN: 9780994606303.

George, D.A., Largies, J.L., Storlazzi, C.D., Barnard, P.L., 2015. Classification of rocky headlands in California with relevance to littoral cell boundary delineation. Marine Geology, 369, 137–152.

George, D.A., Largier, J.L., Pasternack, G.B., Barnard, P., Storlazzi, C.D., Erikson, L.H., 2019. Modeling sediment bypassing around idealized rocky headlands. Journal of Marine Science and Engineering, 7, 40, p. 1–37.

Giorgi, F., Hewitson, B., Christensen, J., Hulme, M., von Storch, H., Whetton, P., Jones, R., Mearns, L. and Fu, C., 2001. Regional climate information—Evaluation and projections. In: Climate Change 2001. The Scientific Basis. Contribution of Working Group to the Third Assessment Report of the IPCC: Contribution to Working Group I, edited by J. T. Houghton et al., chap. 10, p. 583–638, Cambridge Univ. Press, Cambridge, U.K.

Goodwin, I.D., Freeman, R., Blackmore, K., 2013. An insight into headland sand bypassing and wave climate variability from shoreface bathymetric change at Byron Bay, New South Wales, Australia. Marine Geology, 341, p. 29–45.

Goodwin, I.D., Ribo, M., Mortlock, T., 2020. Coastal sediment compartments, wave climate and centennial-scale sediment budget. In: Jackson, D., Short, A.D. (Eds.), Sandy Beach Morphodynamics, vol. 2020. Elsevier, 814p.

Graffin, M., Almar, R., Boucharel, J., Abessolo, G.O., Thoumyre, G., Papa, F., Montaño, J., Bergsman, E.W.J., Baba, M.W., Jin, F-F., Ranasinghe, R., pre-print. El Niño controls the evolution 1 of shorelines worldwide. Research Square, https://doi.org/10.21203/rs.3.rs-1283693/v1

Gray, J.L., Verdon-Kidd, D.C., Callaghan, J., English, N.B., 2020. On the recent hiatus of tropical cyclones landfalling in NSW, Australia. Journal of Southern Hemisphere Earth Systems Science, 70, p. 180–192.

Grothe, P.R., Cobb, K.M., Liguori, G, Di Lorenzo, E., Capotondi, A., Lu, Y., et al., 2019. Enhanced El Niño–Southern oscillation variability in recent decades. Geophysical Research Letters, 46, e2019GL083906.

Grose, M., Timbal, B., Wilson, L., Bathols, J., Kent, D., 2015. The Subtropical Ridge in CMIP5 models, and implications for projections of rainfall in southeast Australia. Australian Meteorology and Oceanography Journal, 65, p.90–106.

Harley, M.D., Turner, I.L., Short, A.D., Ranasinghe, R., 2010. Interannual variability and controls of the Sydney wave climate. International Journal of Climatolology, 30, 9, p. 1322–1335.

Harley, M.D., Turner, I.A., Kinsela, M.A., Middleton, J.H., Mumford, P.J., Splinter, K.D., Phillips, M.S., Simmonds, J.A., Hanslow, D.J., Short, A.D., 2017. Extreme coastal erosion enhanced by anomalous extratropical storm wave direction. Nature Scientific Reports, 7, 6033, p. 1-9.

Harley, M.D., Masselink, G., Alegría-Arzaburu, A. R., Valiente, N.G., Scott, T., 2022. Single extreme storm sequence can offset decades of shoreline retreat projected to result from sea-level rise. Natutre Communications Earth and Environment, 3, 112, p. 1-9.

Hastie, T., Tibshirani, R. and Friedman, J., 2001. The Elements of Statistical Learning: Data Mining, Inference, and Prediction. Springer, 533 p.

Hemer, M.A., Church, J.A., Hunter, J.R., 2010. Variability and trends in the directional wave climate of the southern hemisphere. International Journal of Climatolology, 30, 4, p. 475–491.

Hemer, M.A., Fan, Y., Semedo, A., Wang, X.L., 2013. Projected changes in wave climate from a multi-model ensemble. Nature Climate Change, 3, 471–476.

Hopkins, L.C. and Holland, G.J., 1997. Australian Heavy-Rain Days and Associated East Coast Cyclones: 1958–92. American Meteorological Society, p. 621-635.

Johnson, Z.F., Chikamoto, Y., Wang, S-Y., McPhaden, M.J., Mochizuki, T., 2020. Pacific decadal oscillation remotely forced by the equatorial Pacific and the Atlantic Oceans. Climate Dynamics, 55, p. 789–811.

King, E. V., Conley, D. C., Masselink, G., Leonardi, N., McCarroll, R. J., Scott, T., 2019. The impact of waves and tides on residual sand transport on a sediment-poor, energetic, and macrotidal continental shelf. Journal of Geophysical Research: Oceans, 124, 4974–5002. https://doi.org/10.1029/2018JC014861.

King, E.V., Conley, D.C., Masselink, G., Leonardi, N., McCarroll, R.J., Scott, T., Valiente, N.G., 2021. Wave, tide and topographical controls on headland sand bypassing. Journal of Geophysical Research: Oceans, 126, e2020JC017053. https://doi.org/10.1029/2020JC017053.

Klein, A.H.F., Vieira da Silva, G., Taborda, R., Silva, A.P., Short, A.D., 2020. Headland bypassing and overpassing: form, processes and applications. In: Jackson, D., Short, A.D. (Eds.), Sandy Beach Morphodynamics, 2020. Elsevier (814p).

Kossin, J.P., Emmanuel, K.A., Vecchi, G.A., 2014. The poleward migration of the location of tropical cyclone maximum intensity. Nature – Letter, 509, p. 349-352.

Li, S., Wu, L., Yang, Y., Geng, T., Cai, W., Gan, B., Chen, Z., Jing, Z., Wang, G., Ma, X., 2020. The Pacific Decadal Oscillation less predictable under greenhouse warming. Nature Climate Change, 10, p. 30-34.

Lobeto, H., Menendez, M., Losada, I.J., 2021. Projections of directional spectra help to unravel the future behavior of wind waves. Frontiers in Marine Science, 8, 655490, doi: 10.3389/fmars.2021.655490.

Lopez, H., Lee, S-K., Kim, D., Wittenberg, A.T., Yeh, S-W., 2022. Projections of faster onset and slower decay of El Niño in the 21st century. Nature Communications, 13, 1915, p. 1-13.

McCarroll, R.J., Masselink, G., Valiente, N.G., Scott, T., King, E.V., Conley, D., 2018. Wave and tidal controls on embayment circulation and headland bypassing for an exposed, macrotidal site. Journal of Marine Science and Engineering, 6, 94, p. 1–32. doi:10.3390/jmse6030094.

Montaño, J., Coco, G., Cagigal, L., Mendez, F., Rueda, A., Bryan, K. R., Harley, M. D., 2021. A multiscale approach to shoreline prediction. Geophysical Research Letters, 48, e2020GL090587. https://doi.org/10.1029/2020GL090587

Mortlock, T.R. and Goodwin, I.D., 2015. Directional Wave Climate and Power Variability along the Southeast Australian Shelf. Continental Shelf Research, 98, p.36-53.

Odériz, I., Silva, R., Mortlock, T. R. and Mori, N., 2020. El Niño-Southern Oscillation impacts on global wave climate and potential coastal hazards. Journal of Geophysical Research: Oceans, 125, p.1-16.

Patterson, D., 2007. Comparison of recorded Brisbane and Byron wave climate and implications for calculation of longshore sand transport in the region. In: Proceedings of the 18th Australasian Conference on Coastal and Ocean Engineering, Coasts and Ports 2007, Melbourne, July 2007.

Pérez, J., Mendez, F.J., Menendez, M. and Losada, I.J., 2014. ESTELA: a method for evaluating the source and travel time of the wave energy reaching a local area. Ocean Dynamics, 64, 8, p.1181–1191.

Reguero, B.G., Losada, I.J., Mendez, F.J., 2019. A recent increase in global wave power as a consequence of oceanic warming. Nature Communications, 10, 205, p.1-14.

Ribeiro, M., 2017. Headland Sediment Bypassing Processes Ph.D. Thesis Universidade de Lisboa, Faculdade de Ciencias, Lisbon, 232p.

Ribo, M., Goodwin, I.D., O'Brien, P., Mortlock, T., 2020. Shelf sand supply determined by glacial-age sea-level modes, submerged coastlines and wave climate. Nature Scientific Reports, 10, 462, p. 1-10.

Rueda, A.C., 2013. Statistical downscaling of multivariate wave climate in Gold Coast, Australia. Masters Thesis. Departamento de Ciencias y Tecnicas del Agua y del Medio Ambiente, Universidad de Cantabria, 63p.

Saha, S. et al., 2010. The NCEP Climate Forecast System Reanalysis. Bulletin of the American Meteorology Society, 91, p.1015–1057.

Saha, S. et al., 2014. The NCEP Climate Forecast System Version 2. Journal of Climate, 27, p.2185–2208. https://doi.org/10.1175/JCLI-D-12-00823.1

Shan, K. and Yu, X., 2020. Enhanced understanding of poleward migration of tropical cyclone genesis. Environmental Research Letters, 15, 104062, p. 1-15.

Shand T.D., Goodwin, I.D., Mole, M.A., Carley, J.T., Browning, S., Coghlan, I.G., Harley, M.D., Peirson, W.L., You, Z-J., Kulmar, M.A., 2010. NSW Coastal Storms and Extreme Waves. In: Proceedings of the 19th NSW Coastal Conference. Batemans Bay, NSW, p.1-14.

Short, A. D. 2019. Central East Region (Chapter 18). In: Short, A.D. Australian Coastal Systems – Beaches, Barriers and Sediment Compartments. Springer, Coastal Research Library Series, 1261p., ISBN 978-3-030-14294-0.

Short, A. D., 2022. Australian beach systems: Are they at risk to climate change?. Ocean and Coastal Management, 224, 106180, p. 1-10.

Silva, A.P., Klein, A.H.F., Fetter-Filho, A.F.H., Hein, C.J., Mendez, F.J., Broggio, M.F., Dalinghaus, C. 2020a. Climate-induced variability in South Atlantic wave direction over the past three millennia. Nature Scientific Reports, 10, 18553, p. 1-12.

Silva, A.P.; Vieira da Silva, G.; Strauss, D.; Murray, T.; Woortmann, L.G.; Taber, J.; Cartwright, N.; Tomlinson, R., 2021a. Headland bypassing timescales: Processes and driving forces. Science of the Total Environment, 793, 148591, p. 1-16. https://doi.org/10.1016/j.scitotenv.2021.148591.

Silva, A.P.; Gomes da Silva, P.; Vieira da Silva, G.; Perez, J.; Cagigal, L.; Murray, T.; Strauss, D. and Tomlinson, R. 2021b. Wave Generation Zones off the East Australian Coast. In: (Conference Paper) Proceedings of the Australasian Coasts and Ports 2021, Christchurch – New Zealand, 30 November to 03 December 2021, p.1-7.

Speer, M., Leslie, L., Hartigan, J., MacNamara, S., 2021. Changes in Frequency and Location of East Coast Low Pressure Systems Affecting Southeast Australia. Climate, 9, 44. https://doi.org/10.3390/cli9030044

Splinter, K.D., Davidson, M.A., Golshani, A., Tomlinson, R., 2012. Climate controls on longshore sediment transport. Continental Shelf Research, 48, 146–156.

Splinter, K.D. and Coco, G., 2021. Challenges and Opportunities in Coastal Shoreline Prediction. Frontiers in Marine Science, 8, 788657, doi: 10.3389/fmars.2021.788657

Strauss, D., Burston, J., Girondel, T., Tomlinson, R., 2013. Multi-decadal analysis of profile response to permanent bypassing. Coastal Dynamics, p.1547-1558.

Thom, B.G., Eliot, I., Eliot, M., Harvey, N., Rissik, D., Sharples, C., Short, A.D., Woodroffe, C.D., 2018. National sediment compartment framework for Australian coastal management. Ocean and Coastal Management, 154, p. 103–120.

Valiente, N.G., Masselink, G., Scott, T., Conley, D., McCarroll, R.J., 2019. Role of waves and tides on depth of closure and potential for headland bypassing. Marine Geology, 407, p. 60–75.

Valiente, N.G., Masselink, G., McCarroll, R.J., Scott, T., Conley, D., King, E., 2020. Nearshore sediment pathways and potential sediment budgets in embayed settings over a multi-anuual timescale. Marine Geology, 427, p. 1–19.

Van Rijn, L.C., Walstra, D.J.R., Grasmeijer, B., Sutherland, J., Pand, S., Sierra, J.P., 2003. The predictability of cross-shore bed evolution of sandy beaches at the time scale of storms and seasons using process-based profile models. Coastal Engineering, 47, p.295-327.

Vieira da Silva, G., Muler, M., Prado, M.F.V., Short, A.D., Toldo Jr., E.E., Klein, A.H.F., 2016a. Shoreline changes analysis and insights into sediment transport path - example of Santa Catarina Island North Shore, Brazil. Journal of Coastal Research, 32, 4, p.863-874.

Vieira da Silva, G., Toldo Jr., E.E., Klein, A.H.F., Short, A.D., Woodroffe, C.D., 2016b. Headland sand bypassing - quantification of net sediment transport in embayed beaches, Santa Catarina Island North Shore, Southern Brazil. Marine Geology, 379, p.13-27.

Vieira da Silva, G., Toldo Jr., E.E., Klein, A.H.F., Short, A.D., Tomlinson, R., Strauss, D., 2017. A Comparison between natural and artificial headland sand bypassing in Santa Catarina and the Gold Coast. In: Proceedings of Australiasian Coasts and Ports 2017 (Cairns, Queensland), p.1-7.

Vieira da Silva, G., Toldo Jr., E.E., Klein, A.H.F., Short, A.D., 2018a. The Influence of Wave-Wind- and Tide-Forced Currents on Headland Sand Bypassing – Study Case: Santa Catarina Island North Shore, Brazil. Geomorphology, 312, p.1-11.

Vieira da Silva, G., Murray, T. and Strauss, D., 2018b. Longshore wave variability along non-straight coastlines. Estuarine, Coastal and Shelf Science, 212, p.318-328.

Vieira da Silva, G., Strauss, D., Murray, T., Tomlinson, R., Silva, A.P., Faivre, G., Elliot-Perkins, Z., Wharton, C., Prenzler, P., Hemer, M., 2021. Impacts of Climate Change on Sediment Transport Rates Around Burleigh Heads. In: (Conference Paper) Proceedings of the Australasian Coasts and Ports 2021, Christchurch – New Zealand, 30 November to 03 December 2021, p.1-7.

Vos K., Harley M.D., Turner I.L., Splinter K.D., pre-print. Large regional variability in coastal erosion caused by ENSO. https://doi.org/10.21203/rs.3.rs-666160/v1

Wiggins, M., Scott, T., Masselink, G., McCarroll, R.J., Russell, P., 2020. Predicting beach rotation using multiple atmospheric indices. Marine Geology, 426, 106207, p. 1–12.

Wishaw, D., Leon, J., Fairweather, H., Crampton, A., 2021. Influence of wave direction sequencing and regional climate drivers on sediment headland bypassing. Geomorphology, p. 1–18.

Yang, H., Lohmann, G., Lu, J., Gowan,E. J., Shi, X., Liu, J., & Wang, Q., 2020.Tropical expansion driven by poleward advancing midlatitude meridional temperature gradients. Journal of Geophysical Research: Atmospheres, 125, e2020JD033158. https://doi.org/10.1029/2020JD033158

Zarifsanayei, A.R., Antolínez, José.A.A., Etemad-Shahidi, A., Cartwright, N., Strauss, D., 2022. A multi-model ensemble to investigate uncertainty in the estimation of wave-driven longshore

1138 sediment transport patterns along a non-straight coastline. Coastal Engineering, 173, 104080, p.
1139 1-17. doi:https://doi.org/10.1016/j.coastaleng.2022.104080.